REVIEWS OF

MODERN PHYSICS

VOLUME 28, NUMBER 2 APRIL, 1956

Monoenergetic Neutron Techniques in the 10- to 30-Mev Range*

J. L. FOWLER, *Oak Ridge National Laboratory, Oak, Ridge, Tennessee*

AND

JOHN E. BROLLEY, JR., *Los Alamos Scientific Laboratory, University of California, Los Alamos, New Mexico*

A review is given of the techniques for detection of 10- to 30-Mev monoenergetic neutrons with emphasis being placed on absolute neutron flux measurements. Charged particle reactions, which result in monoenergetic neutrons, are discussed; the published cross-section data for the neutron producing reactions involving the hydrogen isotopes are collected and presented as a function of energy and angle. Sources of background neutrons are considered. Tables of neutron energies including relativistic effects for the hydrogen isotope reactions are presented.

INTRODUCTION

THIS review of cross sections and techniques for neutron measurements in the 10- to 30-Mev region was started in 1953 at the request of the Subcommittee on Neutron Measurements of the National Research Council.† It was felt that an article was needed to cover this range of neutron energies in a manner similar to the reviews of the lower energy neutron techniques available in several published articles‡ (49H1,§ 50A1, 52B1, 52B2). This review is divided into three main sections: I. Neutron Detection, II. Neutron Sources, and III. Neutron Background. There is some inevitable overlapping of the material covered in previous articles. In particular, the information on cross sections of the neutron producing reactions among the hydrogen isotopes is brought up to date.

Relatively recent theoretical calculations of the cross sections for reactions among the hydrogen isotopes (48K, 49N, 52B3, 50B1, 50P1, 54F1, 51B1, 51F1) have met with considerable success in giving qualitative explanations of the variation of the observed cross sections with energy. The detailed agreement between theory and experiment, however, is such that it was felt for the purposes of experimentalists for whom this review is primarily intended, it would be better to present these cross sections as empirical information.

With a few exceptions, this review included literature references through December, 1954. The system of identifying references is that used for the collection of nuclear data of the National Bureau of Standards (50N).

I. NEUTRON DETECTION

The sources of neutrons we shall consider range from several Mev up to approximately 30 Mev. Various accelerators utilizing a number of reactions involving light nuclei can produce these neutrons. Concomitant with the production of neutrons of desired energy, there often exists copious production of neutrons of other energies. These spurious neutrons will, in many cases, prohibit the use of flat response detectors or total source strength methods. Strong gamma-ray backgrounds may impose additional restrictions on the choice of detection systems. Some methods of detection which cope with such backgrounds may be divided into the following four classes: (1) recoil particle method, (2) secondary standard method (threshold reaction), (3) associated particle method, and (4) time-of-flight method.

---

* Work performed under the auspices of the U. S. Atomic Energy Commission.

† Members of Subcommittee on Neutron Measurements and Standards of the National Research Council include the following: H. H. Barschall, J. H. Coon, D. J. Hughes, L. Turner, A. Wattenberg, J. H. Williams, H. L. Anderson, M. Goldhaber, A. O. Hansen, C. G. Shull, and R. F. Taschek.

‡ See Bibliography at end of article.

§ Professor J. H. Williams has informed us that the ordinate of Fig. 11 is incorrect.

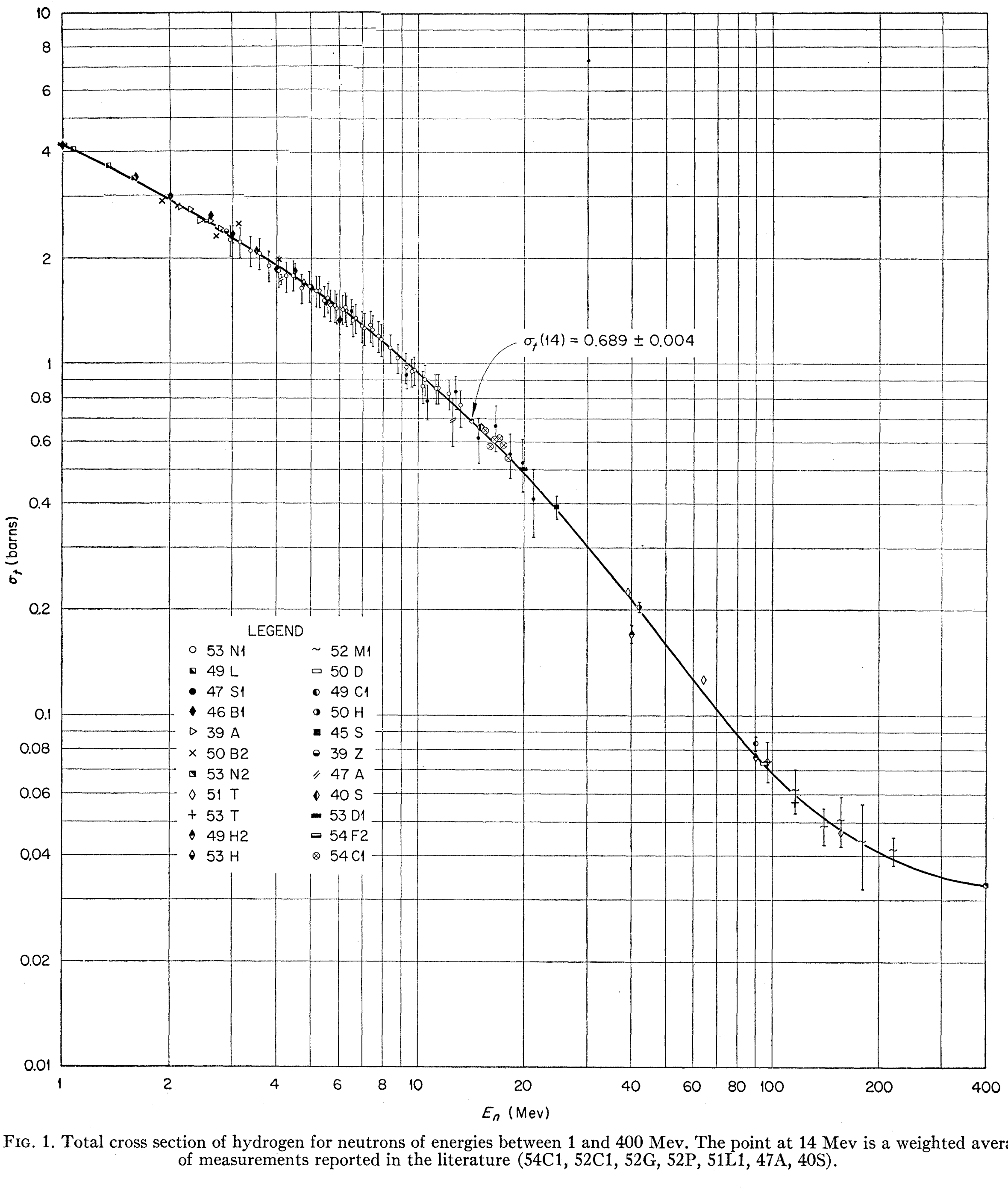

FIG. 1. Total cross section of hydrogen for neutrons of energies between 1 and 400 Mev. The point at 14 Mev is a weighted average of measurements reported in the literature (54C1, 52C1, 52G, 52P, 51L1, 47A, 40S).

Recoil Particle Method

We consider first the recoil particle method and some of the techniques for applying it. In practice the recoiling proton from a neutron collision in a hydrogeneous substance is most commonly used. In general, the detection of the proton is accomplished by a device which is sensitive to protons in a narrow interval of energy whose maximum is the energy of the incident neutron. Such a restriction greatly facilitates discrimination against background processes. However, it does vitiate the application of some techniques which have been used for low-energy *n-p* scattering studies (50A1).

The condition that the recoil protons have essentially the maximum possible energy is satisfied by the small cone of protons recoiling in the direction of motion of the incident neutron. Thus, if quantitative measurements of neutron flux are desired, a knowledge of the differential *n-p* scattering cross section is necessary.

Since n-p collisions in the present range of interest are assumed to be elastic, it is possible to obtain the absolute differential cross section at a given energy by measuring the total cross section and the relative differential cross section. The latter measurement yields the absolute differential cross section by normalizing its integral over a sphere to equal the measured total cross section.

Many measurements of the total n-p cross section have been made (39A, 39Z, 40S, 45S, 46B1, 47A, 47S1, 49C1, 49H2, 49L, 50B2, 50D, 50H, 51L1, 51T1, 52C1, 52G, 52M1, 52P, 53D1, 53H, 53N1, 53N2, 53T, 54C1, 54F2). These measurements do not require an absolute knowledge of neutron flux. They require only the percentage diminution in the strength of a neutron beam when a hydrogeneous scatterer is inserted therein. Such measurements are capable of rather high precision. Figure 1 presents a graphical summary of the data from 1 to 400 Mev. The vertical lines through the points indicate the standard errors of the measurements whenever these are larger than the symbols designating the points. H. H. Barschall (52B2) describes the techniques of such measurements in a review article.

In the center-of-mass system, the precise behavior of the differential n-p scattering cross section is not known. It is quite clear that somewhere above 10-Mev neutron energy, the scattering becomes appreciably anisotropic and that this tendency becomes more marked as the neutron energy increases. Below 10 Mev the scattering process appears to be isotropic (37B1, 37D, 37K, 44C, 46C1, 47P, 51C1).

At what neutron energy anisotropic scattering becomes significant for experimental studies is not quite clear. An early experiment (42A) has shown a marked anisotropy near 14 Mev. A number of later experiments have indicated isotropy for energies between 10 and 14 Mev (42T, 48L, 53R, 55B, 54S4). Recent results at 14 Mev (49B1, 53A1, 55S) indicate only a 5% decrease in the differential cross section in going from 0 to 90°. Experiments above this energy (49B2, 49H2, 51B2, 51B3, 51W, 53R1, 53S1, 54C2, 54S1, 55G1) have unequivocally demonstrated anisotropic scattering. Figure 2 compares the experimentally observed differential cross sections in the range 14 to 100 Mev. The curves for 14 Mev and 18 Mev are least-squares fits to the recent measurements of the form

$$\sigma(\theta)=\sigma_{90°}(1+A\cos^2\theta).$$

The vertical and horizontal lines in Fig. 2 indicate the standard errors and angular spread in cases where these exceed the size of the points. The curves are drawn under the assumption of symmetry about 90° as the situation appears to be at 90 Mev. Relatively recent cloud-chamber measurements including small angle (~10 to 30° in the c.m. system) neutron scattering at 14 Mev indicate that with approximately 20% statistics the n-p angular distribution is symetrical about 90° in the c.m. system (54S4).

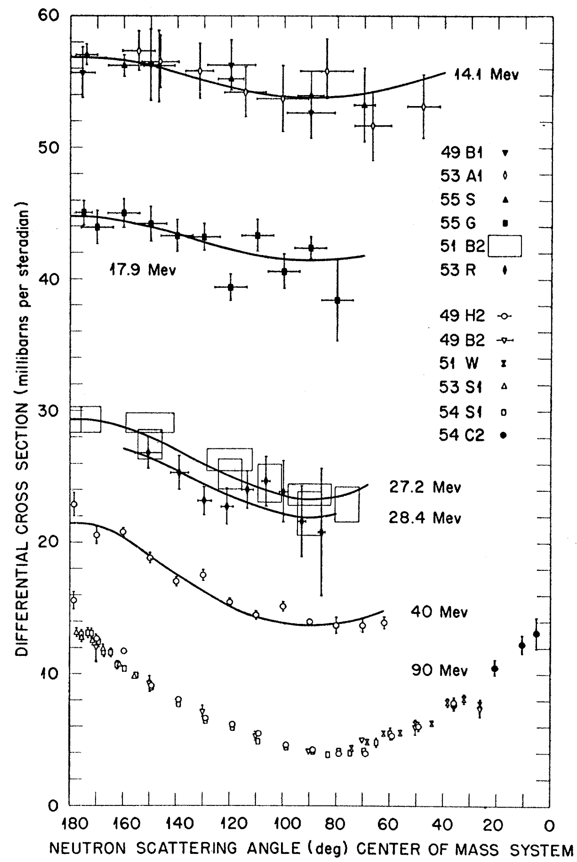

FIG. 2. Differential cross section in c.m. system of neutron proton scattering. Laboratory energy of incident neutrons is given beside each curve. Curves are drawn under the assumption of symmetry about 90°, and are normalized to give total cross sections of Fig. 1. The curves at 14 Mev and at 18 Mev are least-squares fits to the data points.

In Fig. 3 the n-p differential scattering cross section has been converted to the laboratory coordinate system for five proton scattering angles in this system and plotted against neutron energy. Errors are estimated from the uncertainty in the n-p total cross section of Fig. 1, and in the relative differential cross section of Fig. 2. Errors for the possibility of lack of symmetry about 90° were not included. Relativity effects were included in the conversion to the laboratory system (49H2). Below 10 Mev the curves are calculated from the total cross section under the assumption of isotropy in the c.m. system.

A brief summary of the techniques employed in obtaining n-p angular distributions will suggest methods of applying the n-p scattering data. A number of experiments (37B1, 37D, 37K, 48L, 49B2, 51C1, 54S4) have been carried out with the cloud chamber. This technique, which has been adequately described elsewhere (46D), is too cumbersome and time consuming to be used for routine flux measurements. Nuclear emulsions have been used in numerous experiments (44C, 48P, 53A). Here the detector is simple enough

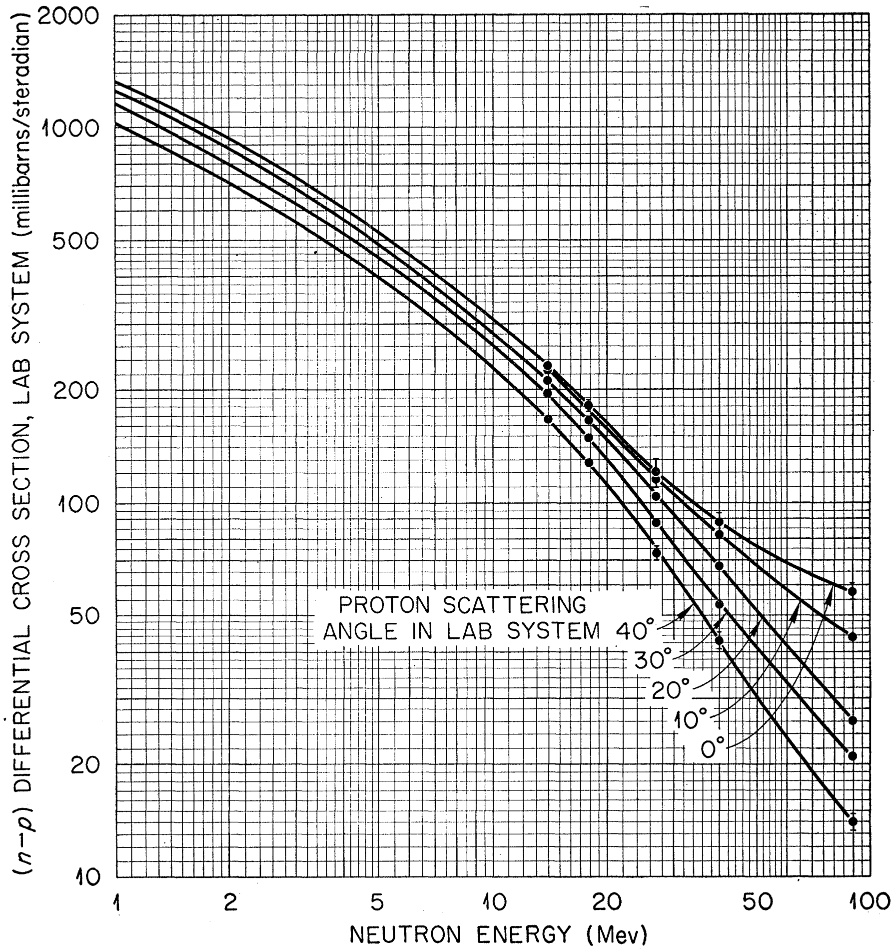

FIG. 3. Laboratory (n-p) scattering cross sections as a function of neutron energy. Points above 10 Mev are taken from Fig. 2 and converted to laboratory system with relativity effects included (49H2). Curves are given for five proton scattering angles in the laboratory system. Errors are estimated from the uncertainty in the (n-p) total cross section and in the relative differential cross sections of Fig. 2. Below 10 Mev the curves are calculated from the total cross section under the assumption of isotropy in the c.m. system.

though the time required to analyze the plates is a disadvantage. Review articles (52B1, 53R2) describe the nuclear emulsion technique in some detail. These two techniques are capable of the best angular resolution because the recoil proton is observed from its point of origin in contradistinction to the methods employing proton radiators of significant dimensions. The nuclear plate method has the additional important advantage of introducing a minimum mass of scattering material in the neutron flux.

Electronic methods in general yield results more rapidly. In this technique detection of protons in a known solid angle or those in a narrow energy interval has been used. It can be shown that in both cases equivalent information is obtained. Where only elastic scattering takes place (n-p scattering is such an example), the number of recoil pulses per unit energy interval plotted against energy gives the differential scattering cross section in the c.m. system as a function of the cosine of the scattering angle (38B, 40B). The recoil pulse height in the counting device must be proportional to the recoil energy or a correction must be applied for the nonlinear pulse height *vs* energy response. In a collision of a neutron with a nucleus of atomic weight A, the nucleus recoils with energy

$$E=\frac{2AE_n}{(1+A)^2}(1-\cos\phi),$$

and an energy distribution

$$P(E)=\frac{\pi\sigma(\phi)}{\sigma_s}\,\frac{(1+A)^2}{A}\,\frac{1}{E_n}dE.$$

Here $P(E)$ is the probability that the nucleus will have a recoil energy between E and $E+dE$; $\sigma(\phi)$ is the differential elastic cross section in the c.m. system for scattering the neutron into the annular solid angle between ϕ and $\phi+d\phi$; σ_s is the total elastic cross section; and E_n is the initial laboratory energy of the neutron. The technique of recoil pulse-height analysis in a gas counter has been limited principally to low-energy neutron measurements (46C1) because of the rapidly increasing range of the recoil protons with energy. Recently the method has been extended to the range 10 to 30 Mev by analyzing the pulse spectrum in hydrogeneous scintillating crystals (52C2, 53R) which generate considerably faster pulses than ordinary proportional counters. Monochromatic neutrons produce an approximately flat differential pulse-height distribution in counters using these crystals. It is possible to obtain some energy discrimination with moderate efficiency. For energies above γ-ray background levels the crystal technique shows promise as a rapid method of measuring monoenergetic neutrons. The angular distribution of n-p scattering at 28 Mev (53R1) was studied by this method. A variation of this technique employs small spheres of organic scintillators embedded in a transparent nonscintillating material to discriminate against γ-ray pulses (54M1).

A more widely used system for the study of the differential cross section consists of a set of proportional counters in tandem (42A, 49B1, 49H2, 51B2, 51B3). The recoil particles traverse the counters and give rise to signals practically coincident in time, whence the recoil particle is counted by observing a coincidence amongst all counters. This arrangement is often given the dubious label "proportional counter telescope." The tandem alignment of the counters restricts the recoil particle beam to a narrow cone. The precise

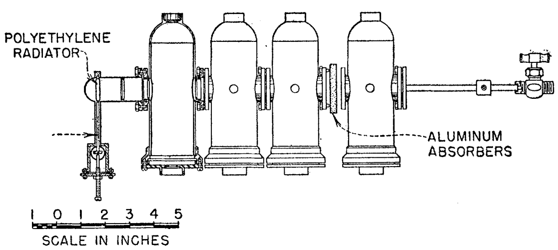

FIG. 4. Fourfold coincidence counter telescope (51B2). Recoil protons from a radiator pass through three proportional counters and the Al absorber and thence into the fourth counter. Fourfold coincidences are required to register a recoil proton.

delimiting is usually accomplished by an aperture placed over the source consisting of a thin film of hydrogeneous material, and an aperture at the entrance of the last counter. Figure 4 is one version of a counter telescope which has been extensively used for neutron flux measurements at Los Alamos (49B1, 51B2). Proton recoils originate in a thin polyethylene film at one end and traverse four platinum lined proportional counters. The platinum liners may be quite thoroughly cleaned of surface contaminants which give rise to spurious particles in the counters under neutron bombardment. Also, being of high Z, relatively few n-p and n-α reactions occur in platinum, thus helping to reduce counter background. Aluminum absorbers of various thicknesses can be inserted between the third and fourth counters to discriminate against recoils below the expected energy interval and to afford a higher bias setting on the fourth counter. The effect of multiple scattering in the absorber must be taken into account. The angular distribution of n-p scattering has been measured at 27 Mev with this apparatus (51B2). This equipment has also been used to measure neutron flux

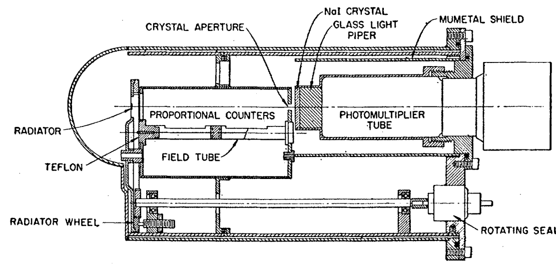

FIG. 5. A threefold coincidence proton recoil telescope (54T). Coincidence pulses from the two proportional counters and the NaI crystal gate a multichannel pulse-height analyzer which measures the pulse height in the NaI crystal. Single-channel pulse-height selectors respond to protons of a given energy loss in the proportional counters, and the NaI crystal measures its residual energy.

in the 10 to 30-Mev region (51B4, 52B4). Argon plus carbon dioxide mixtures, while not as fast as argon plus methane (a source of proton recoils) mixtures, are satisfactory for such counters. This system may be used to delimit the recoil energy more sharply by requiring the particle to stop in the absorber. Electronically this is achieved in the four counters by counting only triple coincidences in the first three counters and imposing an anticoincidence condition between the first three and the fourth (53B1).

An extension of this technique, which permits one to count neutrons having a broad energy spectrum, substitutes a scintillation crystal for the last proportional counter (54R1, 54T). A coincidence amongst all counters generates a gate which activates a pulse analyzer or amplifier in the crystal channel. Figure 5 shows a counter of this type developed at the Oak Ridge National Laboratory by Johnson and Trail which has several advantages for high-energy neutron experiments (54T, 55G1). Such counters have been used to study the anisotropy of n-p scattering at 14 Mev (55S) and at 18 Mev (55G1).

A recent variation of the proportional counter tele-

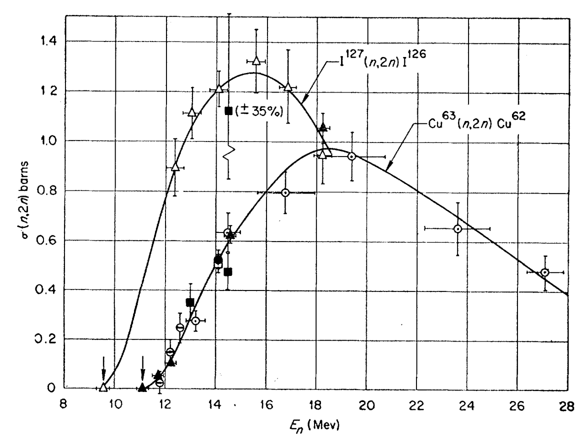

FIG. 6. The $(n,2n)$ cross sections of Cu^{63} and I^{127} as a function of neutron energy. References: △53M, ■53P, ⊙52B4, △52F, ▲52M3, ⊖50F, ●50P2, □50W.

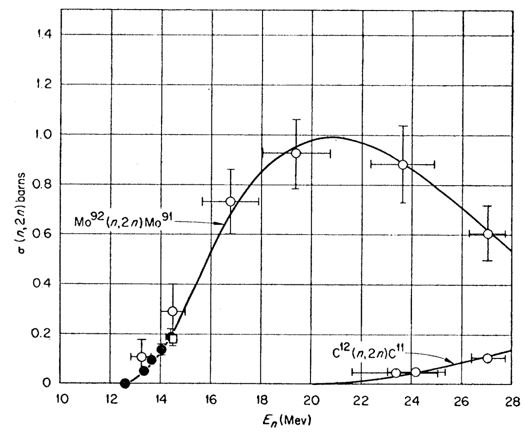

FIG. 7. The $(n,2n)$ cross sections of Mo^{92} and C^{12} as a function of neutron energy. References: ●53B2, ○52B4, □53P.

scope offers improved detection efficiency (52M2). The radiator, as well as the fixed detector, are organic scintillation crystals. A proportional counter lies between the two crystals. The rate of energy loss of the recoil particle traversing the proportional counter serves to identify it. The coincidence pulse from all three counters gates a circuit which measures the sum of the two crystal pulses. From the sum one may obtain the total energy of the recoil proton. Such an arrangement permits use of a relatively thick radiator with higher sensitivity than the "telescope" previously discussed. However, since the scintillators contain only 1/3 the amount of hydrogen per unit volume as the radiators used in the telescope (Fig. 4), the increase in efficiency is not as high as one might at first suppose.

Although protons are most commonly used as recoil particles in neutron detectors, deuterons also find application (53N1). Their use may be occasionally advantageous because of their shorter range and more anisotropic scattering which favors the forward recoil direction. However, appreciable disintegration (55S) of the deuteron occur at 14-Mev neutron energy. About 25% of the total cross section at this energy is represented by disintegration. At lower energies this factor will become inconsequential; experimental knowledge of the disintegration cross section is quite meager.

Secondary Standard Threshold Reaction Methods

Measured neutron reaction cross sections may be used for the absolute determination of neutron flux. This is, of course, a method of secondary standards

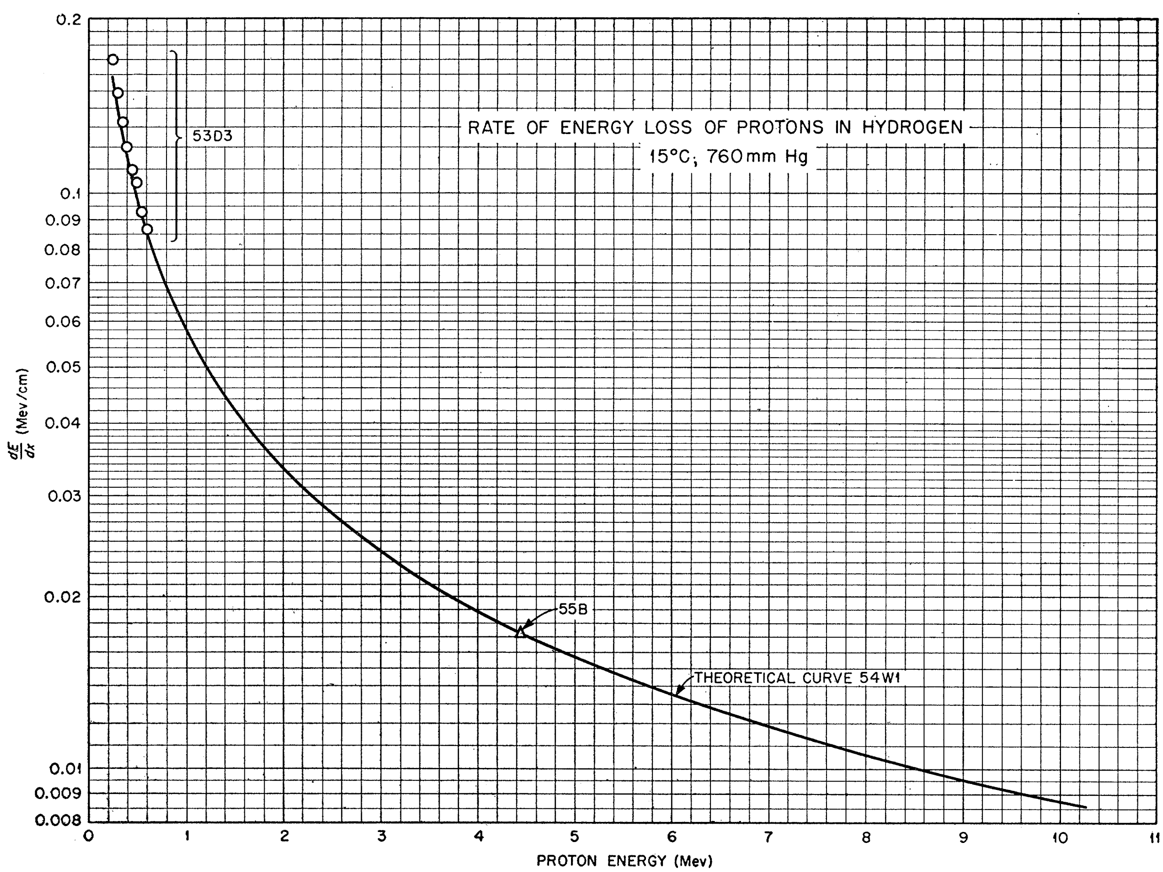

FIG. 8. Rate of energy loss of protons in hydrogen. Open circles (53D3). Open triangle (55B), solid curve theoretical (54W1).

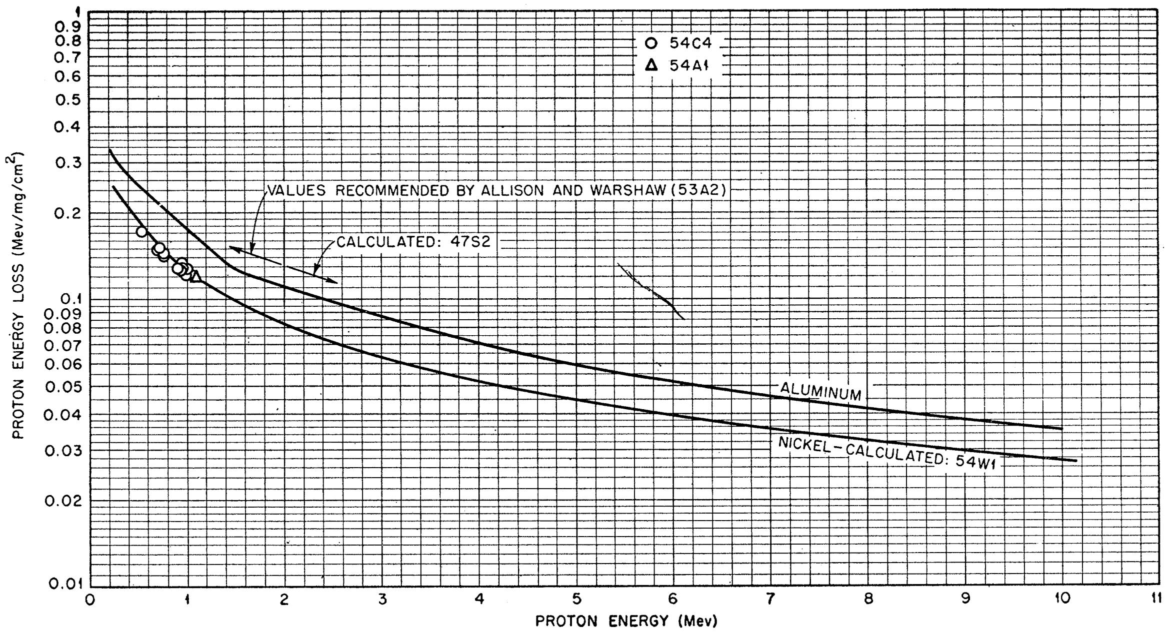

FIG. 9. Rate of energy loss of protons in aluminum and nickel. Aluminum curve (53A2) and (47S2). Nickel curve: ○54C4, Δ54A1; calculated curve (54W1).

since the initial determination of the cross section of the nuclear reaction required a knowledge of absolute flux. Thus, the secondary standards are based on either the recoil particle method or the associated particle method which will subsequently be discussed. There exists enough independent measurements of some nuclear reaction cross sections to permit application of this method with a fair degree of confidence. As in the case of *n-p* scattering, the background may be quite important. Thus, it is desirable to utilize reactions with as high a neutron energy threshold as is possible. Since the binding energy of neutrons in most nuclei ranges from 6 to 14 Mev, the $(n,2n)$ reaction often satisfies the requirement of a convenient threshold. However, this reaction is only practicable when it leads to a radioactive product. Since $(n,2n)$ cross sections rise rapidly to values approximating the nuclear geometrical cross sections (52B5), the method will frequently have adequate sensitivity. The half-life and energy of the product β ray may be the governing considerations in a particular experiment.

Figures 6 and 7 are the summation of data for four $(n,2n)$ reactions (50F, 50P2, 50W, 52B4, 52F1, 52M3, 53B2, 53M, 53P). In these cases the absolute reaction cross section has been measured as a function of energy and there is at least one independent check at some energy. Relative cross-section curves in the case of the $Cu^{63}(n,2n)Cu^{62}$ reaction (52M3) and in the case of the $Mo^{92}(n,2n)Mo^{91}$ reaction (53B2) have been normalized to the absolute values of other experiments. A measurement of the $C^{12}(n,2n)C^{11}$ at 90 Mev (48M) is consistent with the low-energy measurement (52B4) as indicated in Fig. 7. Several investigators have measured a large number (∼35) of $(n,2n)$ cross sections at 14 Mev (52F1, 53P). Also, a great deal of work on $(n,2n)$ reactions produced by polyergic sources has been reported (44J, 49J1, 50L, 50W2, 51C2).

In order to use the information in Figs. 6 and 7 to measure absolute neutron flux, it is necessary to determine absolute β disintegration rates. Techniques for such determinations have been described rather thoroughly elsewhere (49B3, 49Z). The references given for Figs. 6 and 7 also include brief descriptions of absolute β counting used in obtaining the data.

Relatively massive and highly efficient detectors utilizing induced radioactivity produced directly in scintillators have also been employed. Thus, the $(n,2n)$ reaction may be used to produce the 13.1-day activity of I^{126} (53M) in a sodium iodide crystal. A reaction of higher threshold, $C^{12}(n,2n)C^{11}$, has similarly been utilized in organic scintillators (51S1). In some cases

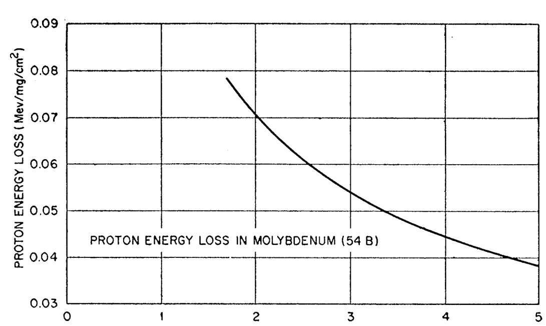

FIG. 10. Rate of energy loss of protons in molybdenum (54B).

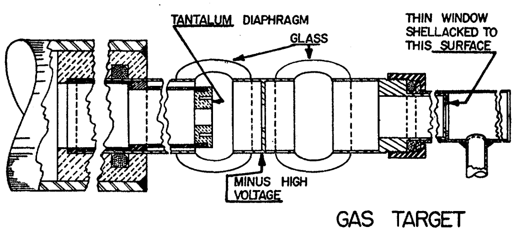

FIG. 11. Target for bombardment of gases (54M2). Beam is delimited by tantalum diaphragm. Target is insulated by glass sections and electrons are returned to source potential by a negatively charged iris. Thin window is shellacked to entrance of gas cell.

the radioactivity may be produced first and then loaded into a scintillator (52D).

Although other threshold reactions such as (n,p) or in some cases (n,α) (53P), and some of the fission reactions (47K, 52A1, 53L) presumably could be used for neutron flux measurements, there is only limited information extant on their energy dependence.

Associated Particle Method

A third detection method, which provides knowledge of absolute neutron flux and energy, utilizes, most commonly, the reactions $D(d,n)He^3$ and $T(d,n)He^4$. The neutrons produced in these reactions have a definite energetic and angular relationship to the charged particles. The angles, of course, are referred to the incident particle beam from the accelerator. The energetics of the process likewise depend on the energy of the accelerated particle. (See Appendices I and II.) At a given angle, the cone of neutrons of known energy will have an associated cone of He^3 or He^4 particle as the case may be. If the neutron background is not too high one measures the neutron flux by counting the associated He^3 or He^4 particles (49G1, 54O). If a high neutron background prevents this and one is interested in some neutron induced prompt process which registers in a counter, coincidences may be taken between this counter and another which detects the associated charged particles (49C2). If the sensitive volume of the associated particle counter encompasses the cone of charged particles corresponding to the cone of neutrons passing through the reactant, its single counting rate will give the flux through the reactant. Hence, the ratio of coincidences to singles gives a direct determination of the reactant cross section when combined with knowledge of the amount of reactant in the neutron flux. Recent advances in high speed counting systems should enhance the usefulness of this technique. Reaction kinematics applicable to this process are presented in Appendix I.

Time of Flight

A fourth method for the detection of neutrons of a given energy imposes the condition that the neutrons lie in a known velocity interval. This method has received considerable application at thermal energies (53E1).

New developments in electronics have permitted the extension of this method to fast neutrons produced by Van de Graaff machines and cyclotrons (54C3, 54O, 54S2). The technique has been employed on a cyclotron (54O) to study the velocity distribution of inelastically

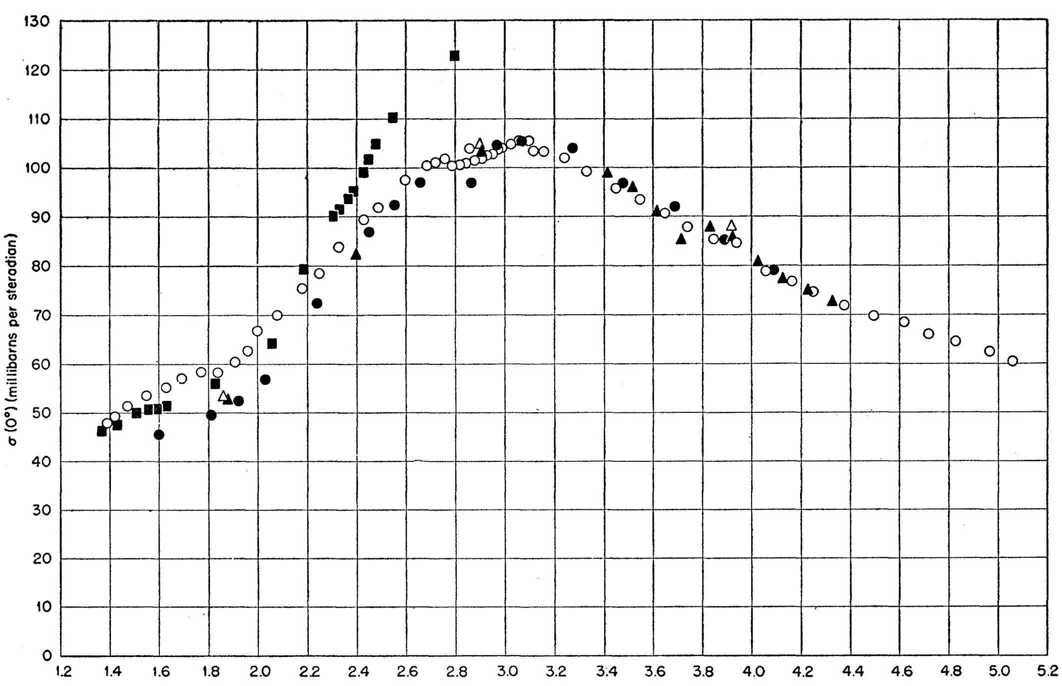

FIG. 12. The differential cross section at 0° for production of neutrons by the $T(p,n)He^3$ reaction (laboratory system). Long counter neutron detection data: Solid circles 54J, solid triangles 54P, open circles 53W, solid squares 50J; stilbene crystal neutron detection data, open triangles 54P.

scattered neutrons. The primary neutrons were produced by the $T(d,n)He^4$ reaction at 100-kev bombarding energy. The associated α particles were detected to furnish a zero time. In the case of Van de Graaff machines (54C3, 54S2) the beam was swept on and off a target by an rf voltage, and the neutrons were detected by organic scintillators. The time interval between the beam pulse and the detection pulse was measured. While the time-of-flight method for fast neutrons is still in an evolutionary state, it is being actively pursued at several laboratories and shows great promise.

II. NEUTRON SOURCES

In general, sources as monoenergetic as possible are desired to facilitate experimental interpretations. This condition imposes a requirement, among others, that the accelerated particle and target nucleus not gives rise to excited states. Practically this is most easily fulfilled by restricting the target nuclei to the hydrogen isotopes and bombarding with protons or deuterons or tritons of various energies. Various combinations of these reactions (except the T+T reaction) have been employed to produce monoenergetic neutrons up to 27 Mev.

$Li^7(p,n)Be^7$ is a prolific source often employed on the Van de Graaff accelerators (49H1). The lithium target is usually in the form of an evaporated layer placed in the accelerator vacuum system. Above 2.4-Mev proton energy a second group of neutrons from the first excited state of Be^7 makes its appearance. For this reason the $Li^7(p,n)Be^7$ source is not useful in the region being

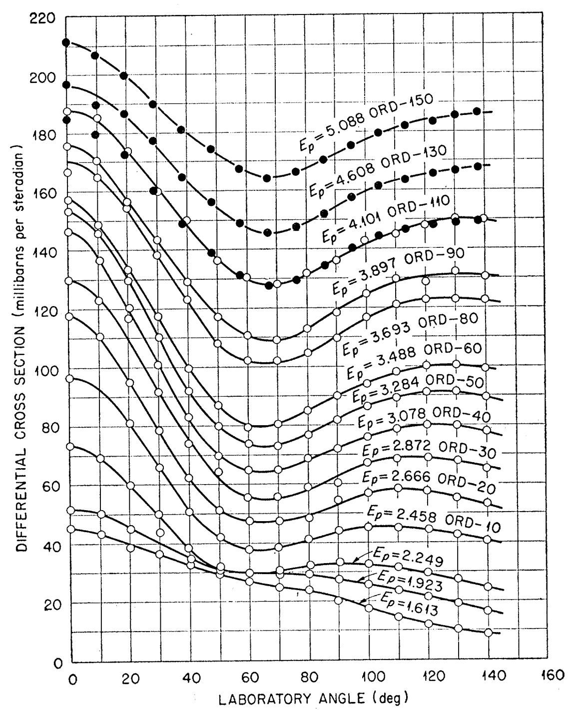

FIG. 14. Differential cross section for neutron production by the $T(p,n)He^3$ reaction as a function of proton energy (laboratory system).

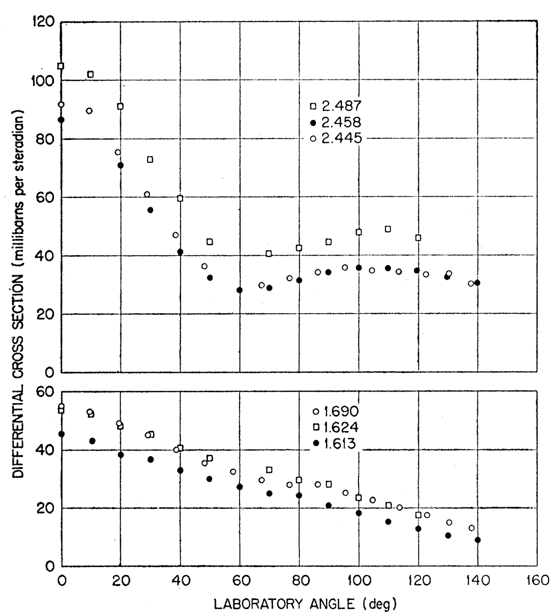

FIG. 13. Comparison of different measurements of laboratory cross sections at selected energies for production of neutrons by the $T(p,n)He^3$ reaction: Solid circles (54J), open circles (53W), open squares (50J).

discussed. In this section we shall consider only the interactions amongst the hydrogen isotopes.

Factors Influencing Monochromaticity

For the reactions we are considering, the spread in energy of the neutrons in a cone at a given angle will be caused principally by geometrical effects and degradation of the energy of the bombarding particles. The geometrical effects arise from the necessity of using finite geometry and are easily calculable from kinematics. Degradation of the bombarding particle will occur during traversal of the thin window, which separates the reaction volume from the accelerator vacuum unless differential pumping is used, and during traversal of the reactant. Concomitant with this process there occurs a second type of geometrical effect which must be taken into consideration in careful work, namely single and multiple scattering in the window and reactant (53D2). Scattering may become quite serious in the case of low-energy bombarding particles and windows of high Z. Degradation of product neutrons may also occur by scattering. This is usually combated by minimizing the amount of material in the environment of the source and detector.

To calculate window and reactant degradation it suffices most commonly to consider the passage of protons through aluminum, nickel, molybdenum, and hydrogen. Aluminum and nickel are by far the most commonly used windows. Since the energy-loss process

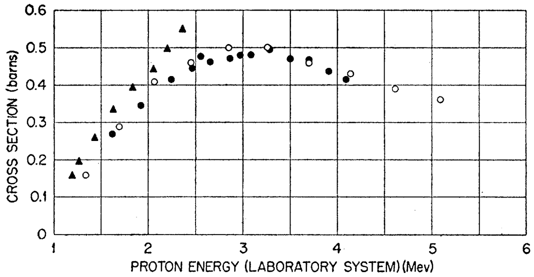

FIG. 15. Total cross section of the $T(p,n)He^3$ reaction as a function of neutron energy: Closed circles (54J), open circles (53W), closed triangles (50J).

is a statistical one, a monoenergetic beam will acquire a small spread in energy as it is degraded. This effect is usually not large for the energy losses of interest here and may be estimated roughly from a formula due to N. Bohr.

$$d\{(E^2)_{Av}-(E_{Av})^2\}=4\pi e^4 z^2 NZdX,$$

where e is the electron charge, z is the charge of the accelerated particle, N is the number of stopping atoms per cc, Z is the atomic number of the stopping atoms, and dX is the path length. If the result is appreciable, Bethe's (53E1) more accurate calculation may be used.

The energy of the accelerated beam, after traversing the window of the reactant vessel, may be calculated quite accurately, providing the initial energy is well known, since the percentage loss of energy in the window is usually small. Several calculations of the rate of energy loss of protons in aluminum have been made (47S2, 51A1).|| In Fig. 8 the proton energy loss is given from 0.25 to 10.0 Mev. Since theoretical calculations of energy loss may be expected to lose accuracy with diminishing energy, the 0.25- to 2-Mev interval has been taken from Allison and Warshaw's (53A2) recommended values. The data have been joined with J. H. Smith's (47S2) calculation to carry the curve to 10 Mev. The range calculated from Smith's dE/dx values at 18 Mev is 2% too low according to Hubbard and McKenzie (52H). Bloembergen and Van Heerden (51B5) find 1 to $1\frac{1}{2}$% higher ranges for protons in the interval 35 to 75 Mev. Figure 9 also presents the calculations of M. C. Walske (54W1) of proton energy loss in nickel. These calculations were normalized to a measurement of H. Argo at 1.089 Mev (54A1). They are in good agreement with the recent measurements of Chilton, Cooper, and Harris (54C4), though systematically slightly higher. Above 1 Mev they cannot be too strongly relied upon because the theory is not strictly valid. More data are needed on nickel.

Molybdenum permits the passage of considerably higher beam currents than aluminum or nickel and moreover is a less copious source of background neutrons. It is, therefore, advantageous in situations where more window scatter and dispersion of beam energy may be tolerated. J. R. Beyster and M. Walt (54B) have measured the rate of energy loss of 3.4-Mev protons in molybdenum by the displaced resonance method. This measurement yielded a value $I=11.87Z$. Figure 10 presents the results of their calculation of dE/dX using this result and values of C_K and C_L (correction factors for binding in K- and L-shells, respectively), suggested by M. C. Walske (54W1).

|| The error alluded to by S. K. Allison and S. D. Warshaw (53A2) in Aron's work appears to be a misprint and did not progagate through the calculations (private communication to F. L. Ribe).

Targets

The target assembly used in a neutron source should be constructed of a minimum amount of material to reduce scattering and be designed for accurate charge

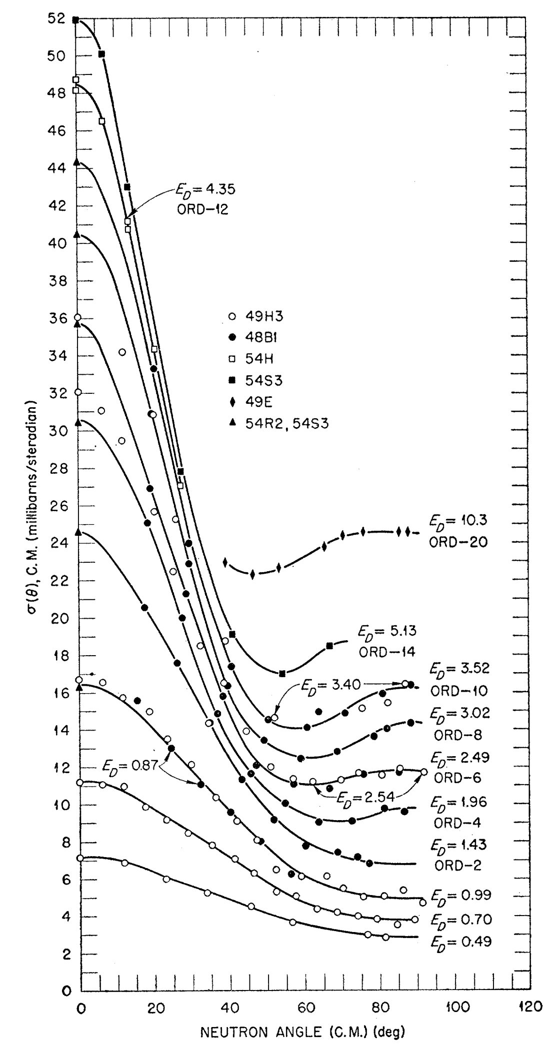

FIG. 16. Differential cross section of the $D(d,n)He^3$ reaction in the c.m. system at various deuteron bombarding energies. Long counter detection of neutrons: (49H3). He^3 detection: (48B1, 49E). Stilbene crystal detection of neutrons: (54H). Proton recoil telescope neutron detection: (54S3). Solid triangle at 0° taken from Fig. 17. (Note shifting ordinate scale.)

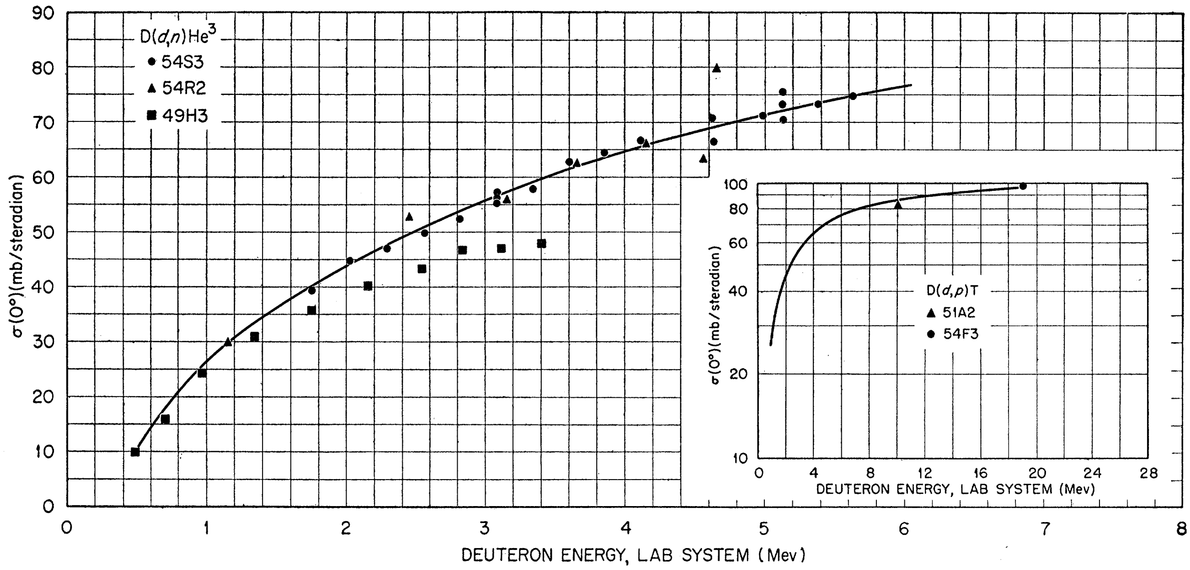

FIG. 17. Laboratory differential cross section at 0° of the $D(d,n)He^3$ reaction to 5.0-Mev deuteron energy and the $D(d,p)T$ reaction in 10- to 20-Mev deuteron energy region.

measurement. Figure 11 illustrates a design of H. C. Martin's which has been used at Los Alamos. The charged particle beam is delimited by a tantalum aperture which may run at a red heat. The elevated temperature inhibits the buildup of carbon and deuterium and this helps to reduce spurious background. Electrons originating at the tantalum aperture and window are forced back to their sources by holding the center iris, which is slightly larger than the beam, a few hundred volts negative with respect to the adjacent structures. Local heating in the beam column in the gas should be kept at a minimum. If this is not done the gross measurements of temperature and pressure will not yield the true number of reactant atoms in the active volume.

$T(p,n)He^3$

Although the endothermic $T(p,n)He^3$ reaction is normally used to produce low-energy neutrons (of a few Mev), it should be applicable for producing monoenergetic neutrons at higher proton energies since He^3 does not appear to have low-lying excited states. The laboratory threshold is $E_p=1.019$ Mev (49T1, 51B6) and the Q-value is -0.764 Mev (54V).

Near threshold the neutrons will emerge in the forword direction in a narrow cone. As the proton energy is increased the cone will open. From formulas in Appendix I we find that at

$$E_p=Q\left\{\frac{(m_1M_1+m_1M_2)}{m_1M_2-m_2M_1}-1\right\}=1.148 \text{ Mev},$$

the cone finally includes all directions. From 1.019 to 1.148 Mev the cone is directed forward and any angle in the cone will have two energy groups of neutrons. The lower energy group, however, will be much less intense.

The various studies of the differential cross section of the $T(p,n)He^3$ reaction (49J2, 50J, 53W, 54J) utilized a common technique. Tritium was bombarded by protons from Van de Graaff generators and neutron yield at various angles and for various proton energies was obtained with a long counter (47H). Calibration of the long counter was performed by exposing it to a flux of neutrons from standard sources such as calibrated RaBe sources. Hence the precision of these measurements is limited by the accuracy of the source calibrations.

Figure 12 shows the measurements of differential cross sections at 0°. The earlier published results are shown as open circles (53W) and solid squares (50J); the latter unpublished results are closed circles (54J). The closed triangles represent data taken with a stilbene crystal counter (54P). The data include the work from two laboratories, Los Alamos Scientific Laboratory (50J, 54J, 54P) and Oak Ridge National Laboratory (53W). Although the Oak Ridge data (open circles) were normalized to the earlier published Los Alamos results (closed squares) at 1.4 Mev, the normalization seems to be the correct one to fit the later Los Alamos results (unpublished, 54J, 54P). Both the Oak Ridge and the later Los Alamos data differ considerably from the earlier Los Alamos data (50J) at higher energies (>2.5-Mev proton energy). The several slight dips in the data are the result of fluctuations of the long counter sensitivity at carbon resonances. The comparison of the angular distributions of three sets of measurements is shown in Fig. 13 (50J, 53W, 54J). Here again the Oak Ridge distributions agree with the earlier Los Alamos measurements at low energies and with the later Los Alamos measurements at higher energies. Since the

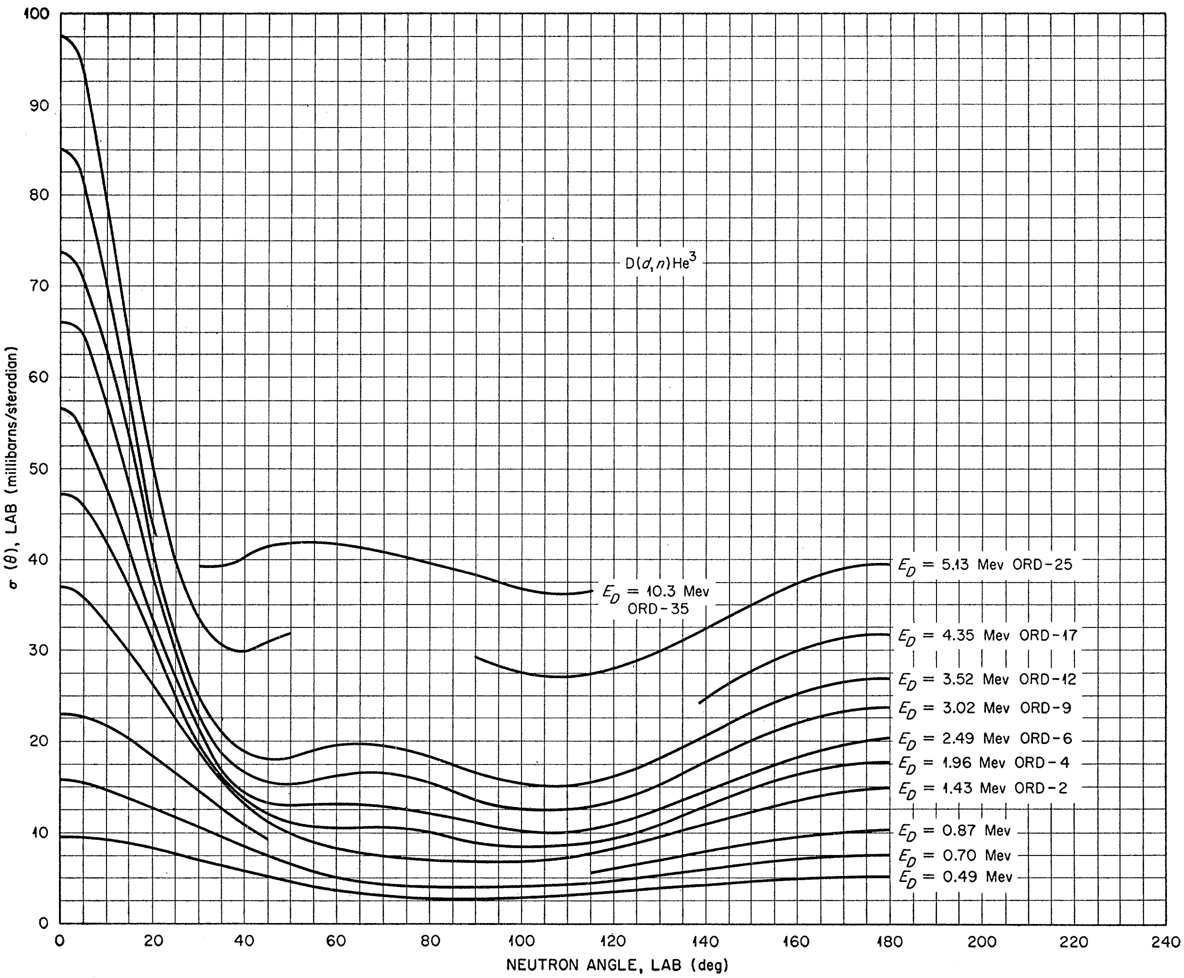

FIG. 18. Laboratory differential cross section of the $D(d,n)He^3$ reaction at various deuteron bombarding energies. Curves obtained by converting data plotted in Fig. 16 to laboratory system.

neutron energy range as a function of angle for the 2.45-Mev proton-energy bombardment overlaps the energy of the neutrons at 0° for the 1.7-Mev proton bombardment, one cannot understand the discrepancy in terms of nonlinearity in energy response of the long counter. At any rate, the two sets of data agree at higher energies so that for the purpose of this paper, one can estimate the cross section to be expected at higher proton energies from the curves of Figs. 14 and 15. Figure 15 shows the total cross section of the $T(p,n)He^3$ reaction as a function of neutron energy. The points are obtained by integrating the differential cross-section data over all solid angles.

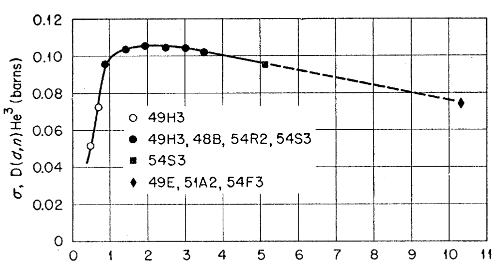

FIG. 19. The total $D(d,n)He^3$ cross section as a function of energy. Curves of Fig. 16 were integrated over all solid angles. The extrapolation of the data in the case of the 5.13-Mev and the 10.3-Mev points introduces an uncertainty in cross section at these energies of 6 and 10%, respectively.

$D(d,n)He^3$

The $D(d,n)He^3$ reaction was the first of the hydrogen isotope reactions to be studied (34O). The early work (35A, 36B, 36K, 36L, 37A, 37L, 37R, 41R, 46M, 50M) was, in general, characterized by low bombarding energies and thick targets. Although some relatively thin target work at higher energies has been reported (46B2), most measurements on this process suitable for precise work at moderate bombarding energies are relatively recent.

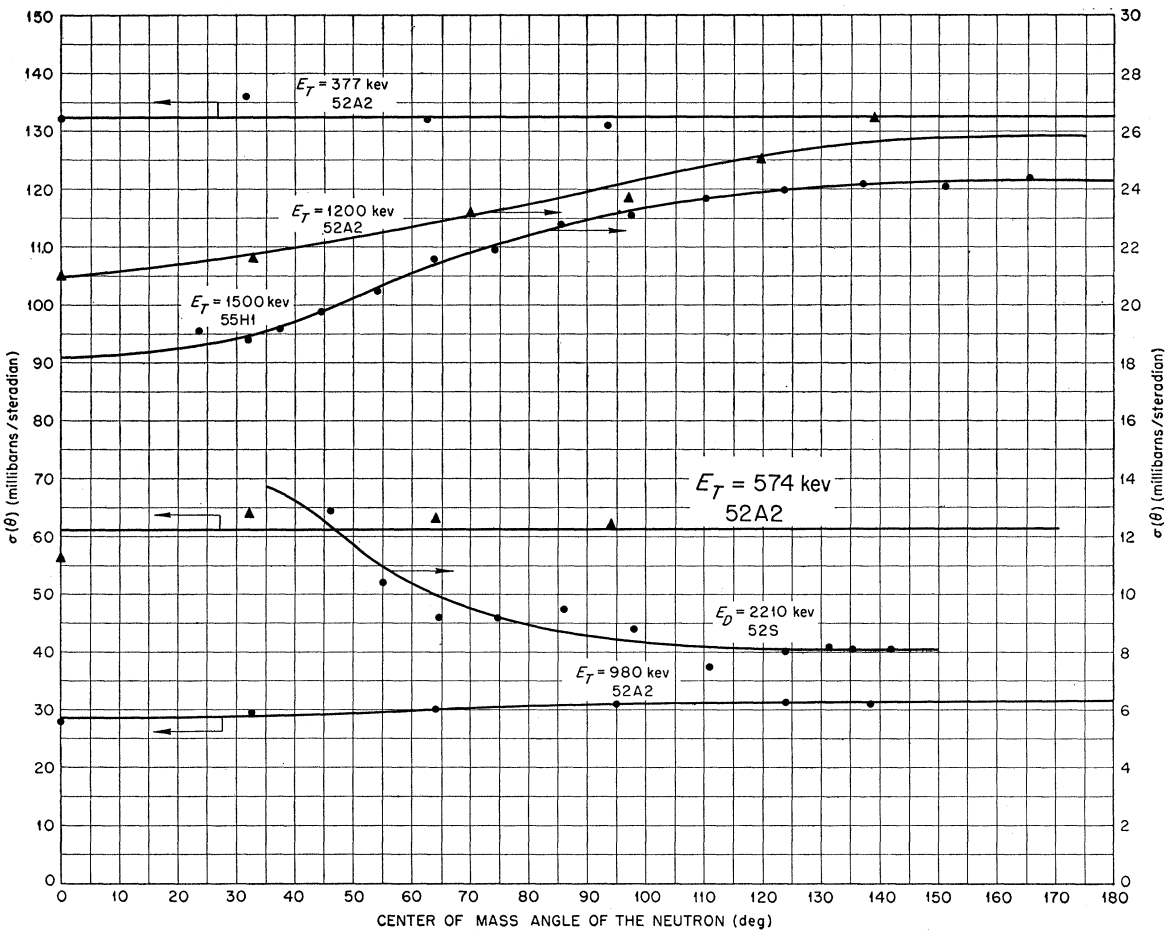

FIG. 20. Differential cross section of the $T(d,n)He^4$ reaction in the c.m. system. The arrows indicate the ordinate to be used for each curve. For all but the 2.21-Mev deuteron bombardment the target was deuterium. The accelerated particles were tritons. For the triton bombardment of 1.5-Mev and the 2.21-Mev deuteron bombardment the associated α particles were counted. The other data were obtained by neutron detection with a long counter.

Hunter and Richards (49H3)¶ have made a detailed study of this reaction for incident deuteron energies from 0.49 to 3.69 Mev produced by a Van de Graaff generator. They measured the neutrons from a gas target with a long counter. The absolute differential cross section for production of He^3 by the $D(d,n)He^3$ reaction, as well as for production of protons from the companion $D(d,p)T$ reaction, has been measured from 1 to 3.5 Mev by Blair, Freier, Lampi, Sleator, and Williams (48B1). In Fig. 16 the differential cross section in the c.m. system of the $D(d,n)He^3$ reaction (48B1) is plotted as solid circles. The statistical accuracy of this data ranged from about 1 to 3%; the authors assign an additional error to the absolute value of 1.7%. Data from Hunter and Richards (49H3) are included where they exist at comparable energies. The maximum statistical error of the latter data was about 5%. Since these data were taken with a long counter calibrated with a RaBe source, there must be an additional uncertainty of the order of 5%. It is evident that over the range of angles of the measurements of Blair *et al.* (48B1) the two independent sets of measurements agree within the limits of error. Recent measurements of the differential cross section at 0° with nuclear emulsions (54R2) and a recoil proportional counter telescope (54S3) give a higher cross section than observed by Hunter and Richards (49H3) see Fig. 17. In Fig. 16 the solid triangles give the 0° differential cross section as read from the smooth curve through the data of Fig. 17.

Also included in Fig. 16 are differential cross-section measurements at higher energies made with a Van de Graaff machine (54H, 54S3) and a cyclotron (49E). For the 4.35-Mev data neutrons were detected with a stilbene crystal (54H); for the 5.13-Mev case, neutrons were detected with a proton recoil telescope (54S3). In the case of the 10.3-Mev cyclotron measurements the product He^3 nuclei were counted (49E).

For an estimate of the differential cross sections at

¶ The abscissa of Fig. 7 is apparently mislabeled as the angles indicated belong to the c.m. system. Professor Richards has informed us that the ordinate of Fig. 3(A) is incorrect.

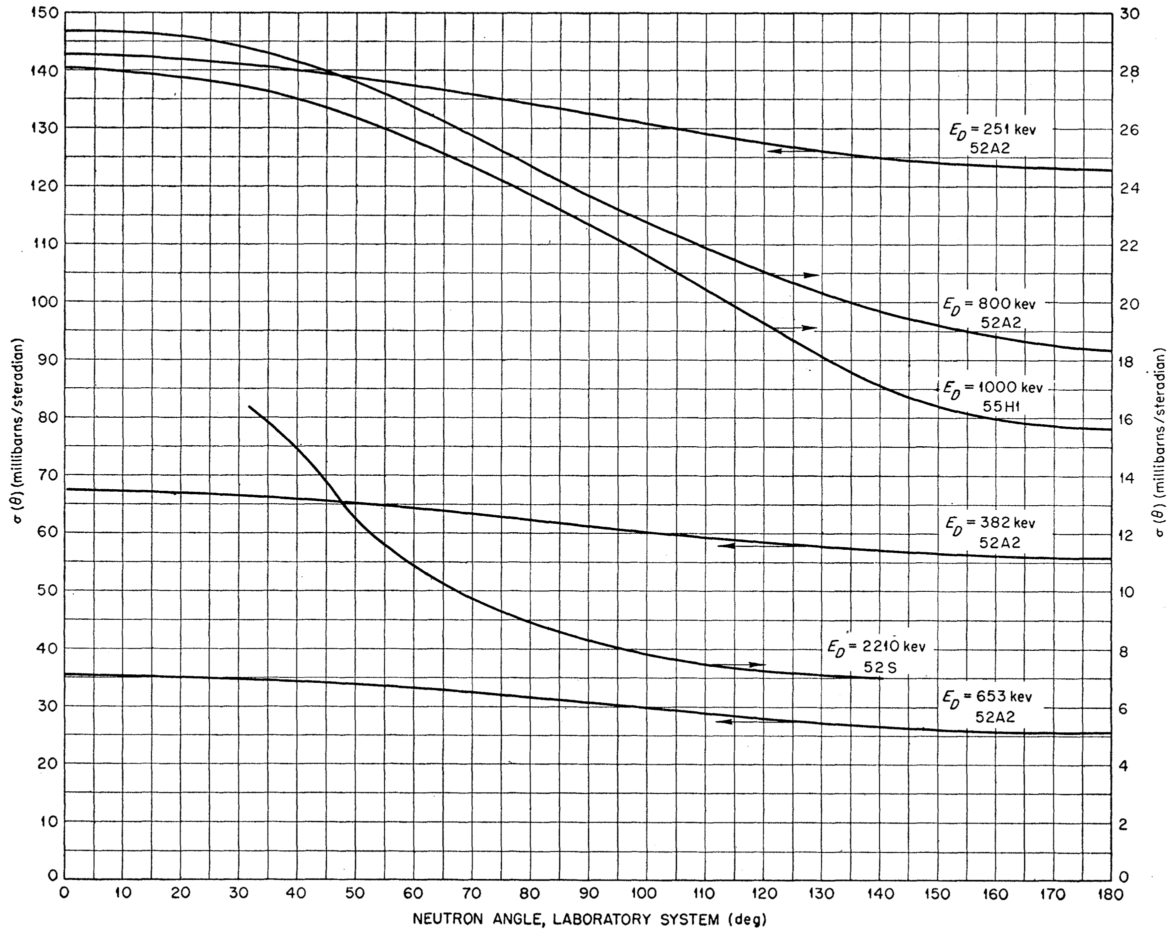

FIG. 21. Differential cross section in laboratory system for neutron production by the T(d,n)He^4 reaction. The arrows indicate the ordinate to be used for each curve. Curves are plotted from data in Fig. 20 and are labeled according to the equivalent deuteron bombarding energy. Estimated error of the 800-, 653-, 382-, and 251-kev curves is $\pm10\%$ (51A2). The 1000-kev data have an error of $\pm3\%$ (55H1), and the 2210-kev data have an error of $\pm8\%$ (52S).

higher energies and at angles not given in Fig. 16, one use the measurements of the D(d,p)T differential cross sections which have been made at 10.3 Mev (51A2) and at 19.1 Mev (54F3). At lower energies (48B1) the cross section for production of neutrons by the *d-d* reaction is very similar to that for the protons. The insert in Fig. 17 shows the estimated extrapolation of the 0° differential cross section as obtained from the D(d,p)T reaction.

In Fig. 18 the c.m. cross sections and angles of Fig. 16 are given in the laboratory system. Figure 19 shows the total cross section of the D(d,n)He^3 reaction as a function of bombarding energy. Below 4 Mev the total cross section should be good to 3%. Mainly because of the uncertainty in extrapolating the data for the 5.13- and 10.3-Mev points, the errors for these points are estimated to be 6 and 10%, respectively.

D(t,n)He^4

Neutrons of energies up to 27 Mev have been supplied by the D+T reaction. The very high Q of this reaction, 17.578 Mev (54V), makes possible the production of such energies with relatively low input energy.

A number of low-energy studies (43B, 49B4, 49T2, 50A2, 52C3, 54A3) exist of this process. Argo *et al.* (52A2) have bombarded deuterium with tritons accelerated by a Van de Graaff machine. They find deuterium targets more advantageous than tritium targets. Angular distributions of the neutrons were obtained with a long counter for triton energies $E_T=380$, 570, 980, 1206 kev. Estimates of room scatter were obtained by the shadow cone technique. In Fig. 20 their results are presented in the c.m. system. These measurements are estimated to have an accuracy of $\pm10\%$.

Hemmendinger and Argo (55H1) have recently made a precise measurement of the α particles from this reaction with a proportional counter for $E_T=1.5$ Mev. This result is also presented in Fig. 20. They assign a probable error of 3% to these data.

Stratton and Freier (52S) have bombarded tritium with deuterons of 2.21 Mev and measured the associated α particles with a proportional counter. Their results are also presented in Fig. 20. They estimate an error of $\pm 8\%$ for their data. In Fig. 21 the data from Fig. 20 are plotted in the laboratory system; the curves are labeled according to the equivalent deuteron bombarding energy.

Total cross sections from these experiments are plotted in Fig. 22. Below 400-kev deuteron energy, the differential cross section in the c.m. system is found to be practically isotropic (49B4, 50A3, 52A2), so that one can calculate the total $T(d,n)He^4$ cross section from differential cross sections obtained at any angle. Several thin target measurements of the differential cross section for emission of α particles at 90° have been made (50A2, 52C3, 54A3). The early experiment by Allan and Poole (50A2) was based on finding the ratio of the $T(d,n)He^4$ cross section at 90° to that of the $D(d,p)T$ reaction. Since the early $D(d,p)T$ cross sections, which Allan and Poole used, were obtained from thick target yields (46G, 48B2, 48F), and differ somewhat from later thin target measurements (48B1, 50S, 54A3), the Allan and Poole data (50A2) have been omitted from Fig. 22. Earlier cross sections of the $T(d,n)He^4$ reaction in the low-energy region (49B4) were obtained by differentiating thick target yields and differ considerably from the data presented here. The data of Conner *et al.* (52C3), designated by crosses in Fig. 22, were obtained with thin zirconium tritide targets (51L2). The authors' estimate of the error was about $\pm 1.5\%$ but they assign an error of about $\pm 3.0\%$. The errors of the other data in Fig. 22 are mentioned elsewhere in this section.

The cross sections of Argo *et al.* (52A2) do not extrapolate as close to the value of Hemmendinger and Argo (55H1) as might be expected from the errors quoted. The former data, which are based on long counter measurements, appear to be low compared with Hemmindinger and Argo's work based on α counting.

At $E_D = 10.5$ Mev, Brolley, Fowler, and Stovall (51B4) have studied this reaction by neutron counting using proton recoils and the $(n,2n)$ reaction and by α counting with a proportional counter. Their results are illustrated in the c.m. plot of Fig. 23. The data of Allred (51A3) on the mirror reaction $He^3(d,p)He^4$ at $E_D = 10.3$ Mev are also presented to illustrate the similarity at this deuteron energy. Stratton and Freier's data (52S) at $E_D = 2.21$ Mev are also compared with the mirror reaction measurement of Yarnell, Lovberg, and Stratton (53Y). At the lower energy disparity is noted. A smoothed curve of the 10.5-Mev data (51B4) in the laboratory system is presented in Fig. 24. The region 139 to 74°, obtained from α counting, has an accuracy of about $\pm 3.5\%$. The region 74 to 0°, obtained by neutron counting, has an error of the order of $\pm 11\%$.

Very many experiments with 14-Mev neutrons have used the $T(d,n)He^4$ reaction at low-deuteron bombarding energy (a few hundred kev) (49B1, 50P2, 52C1, 52F1, 52G, 52P, 53A1, 54C1, 55S). Here the low

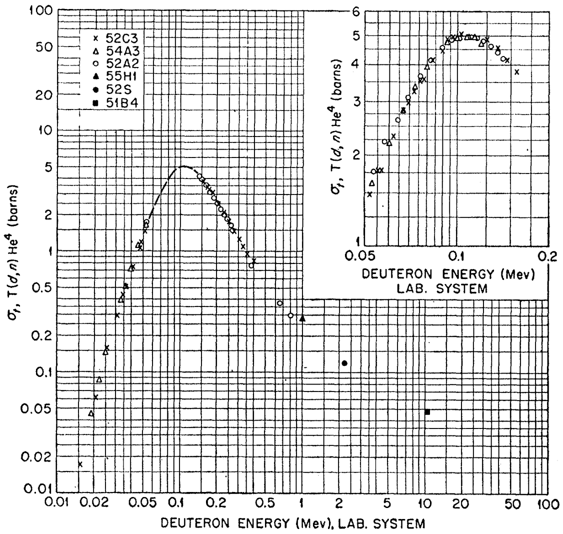

FIG. 22. The total cross section for the $T(d,n)He^4$ reaction as a function of deuteron bombarding energy. The crosses (52C3) and open triangles (54A3) are results of counting alphas at 90° to the deuteron beam. Below $\sim$400 kev the c.m. differential cross section is practically isotropic (Fig. 20). The open and solid circles, solid triangles, and solid squares are data from Figs. 20 and 23.

deuteron energy makes the use of the type of window discussed in the previous section impractical. A very important technique has been developed to provide tritium targets for this energy range (49G1). Tritium gas is absorbed in Zr or Ta metal at relatively high temperatures. In the case of Zr metal, which has proved to be most useful, the Zr foil is fixed to a tungsten or platinum backing (49G1). Very thin ($\sim$10 $\mu g/cm^2$) Zr layers have been prepared by evaporating the Zr metal upon a backing material (51L2). Ratios of hydrogen isotope to Zr or Ta atoms of about 1.0 to 1.5 have been obtained. These targets are relatively stable under long deuteron bombardments. The neutron intensity can be monitored by counting the associated particle, He^4, produced by the d-T reaction (49G1).

Breakup of the Deuteron

Hitherto many experiments employing the hydrogen isotope reactions have relied on the assumption that breakup of the deuteron does not proceed at a significant rate. J. H. Gammel (53G) has observed the breakup of deuterons when bombarded with protons of 9.7 Mev. This corresponds to background measurements in some experiments where the isotope being bombarded by deuterons has been replaced with hydrogen. In general, the breakup neutrons will be of lower energy than those from the primary source and, therefore, in many experiments, but not all, can be discriminated against.

The d-T reaction has been observed to furnish breakup neutrons when the incident deuteron energy in the c.m. system exceeds the deuteron binding energy

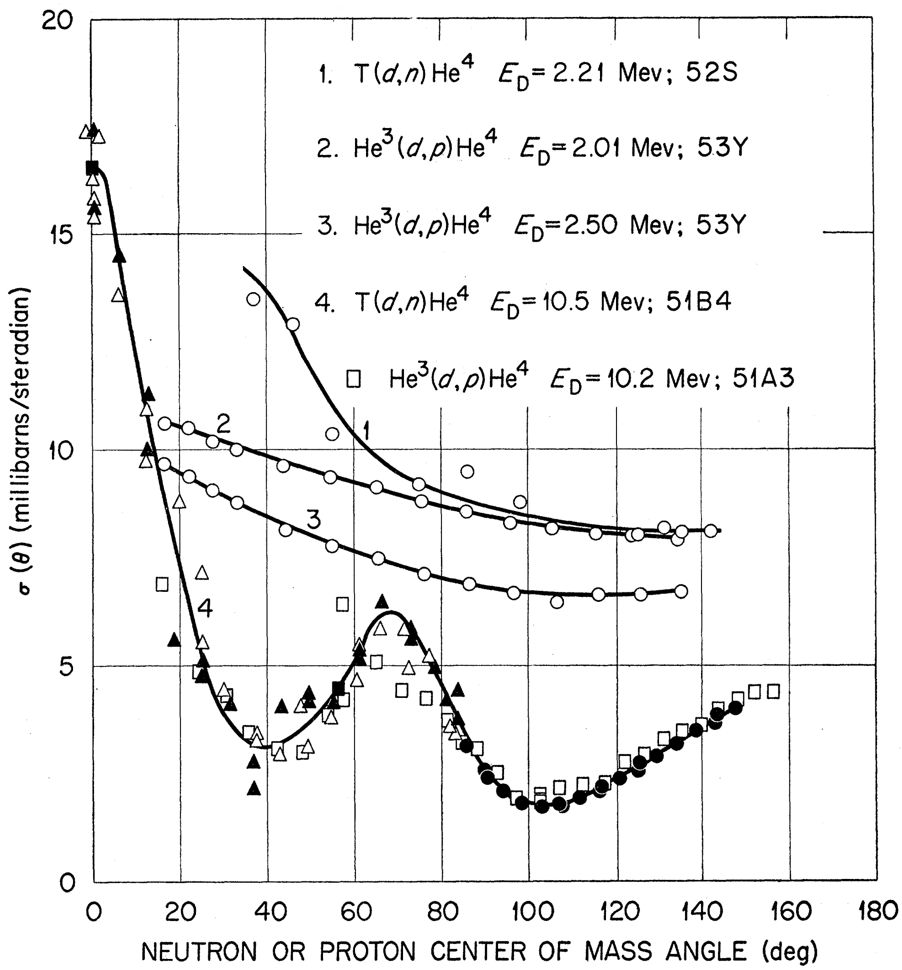

FIG. 23. Center-of-mass differential cross section of T(d,n)He^4 and the He$^3(d,p)$He^4 reaction at higher energies. Neutron detection [telescope and Cu$(n,2n)$] for triangle points. Rest of data; charged particle detection.

(55H2). The yield, which is probably a low-energy continuum, rises rapidly with increasing deuteron energy. The same study, however, indicates that the d-D reaction does not generate breakup neutrons at a significant rate for deuteron energies up to 7 Mev.**

These results emphasize the desirability of using the associated particle method where applicable or some other form of energy discrimination.

Polarization

In the last decade some attention has been directed to the production of polarized neutrons and charged particles. Wolfenstein (49W), Blin-Stoyle (51B7), Simon and Welton (52S2, 53S3), and Fierz (52F2) have considered the theoretical aspects of nuclear reactions as sources of polarized particles. Polarization will not occur if only S-waves of the incident particle are involved in the reaction. However, for the energy interval of interest in this discussion, higher order angular momenta are involved. Simon and Welton (53S2), in their general formulation of the problem, have shown that the polarization of the emitted particle is always normal to the plane defined by the paths of the incident and emitted particle. Moreover, the polarization is always zero for axially emitted particles.

Thus, in the neutron sources we have been describing, the use of nonaxial neutrons must be accompanied by consideration of the effect of polarization of the neutrons on the secondary reaction or process involving the neutrons. In some cases no effects would be expected as, for example, the production of induced radioactivity with nonaxial neutrons. In other cases, such as scattering, the angular distribution of the products of the secondary reaction may be influenced.

Experimental studies of the polarization of nonaxial neutrons are, as yet, rather few. In the Li$^7(p,n)$Be^7 reaction, Adair *et al.* (54A2) have demonstrated a polarization of 0.5 at $E_p=2.262$ Mev and $\theta=50°$ (Lab). Willard *et al.* (54W2) have measured this polarization from $E_p=2.13$ to 2.39 Mev at 42° (Lab) and find that the Li(p,n) neutrons are approximately 50% polarized. The d-D reaction has been examined by Bishop *et al.*

** *Note added in proof.*—Some recent time-of-flight neutron measurements on the breakup of the deuterons in the (d,d) reaction indicate a more prolific yield of breakup neutrons than was earlier anticipated (L. Cranberg and R. L. Henkel, LASL, private communication).

(52B6). For deuterons of 300-kev energy incident on a heavy ice target, they found a proton polarization of 0.3. Polarization of the neutron branch has been observed by using carbon scatterers by Baumgartner and Huber (53B3) and with lead scatterers by Longley, Little, and Slye (52L). Neutron polarization at 45° (c.m.) was observed to be of the order of 20 to 40% for deuterons near 0.5 Mev. For $E_D = 600$ kev, Meier *et al.* (54M3) find a maximum polarization of the *d*-D neutrons of 10.8±1.2% at 58° and 122° (c.m. angles). The neutron experiments are rendered difficult by severe background problems. For T(*p*,*n*) neutrons only fragmentary information exists with regard to polarization. At a laboratory angle of 50° and a proton energy of 1.46 Mev the polarization was found to be essentially 0; 1±4% (54W2). Due consideration for polarization should be given to these reactions when their angular distributions depart from isotropy in the c.m. system.

III. NEUTRON BACKGROUND

Neutron backgrounds may be divided into two groups. The primary neutron background arises from scattering of the primary source neutrons by air and environmental structures into the detector. The secondary neutron background arises from the direct and scattered neutrons generated in the accelerator, beam plumbing, collimators, target windows, and beam stoppers, passing through the detector. In first approximation the primary background may be measured by interposing a shadow bar between the primary neutron source and detector. The secondary background may be obtained in first approximation by removing the primary source reactant. More refined procedures may be required in some experiments.

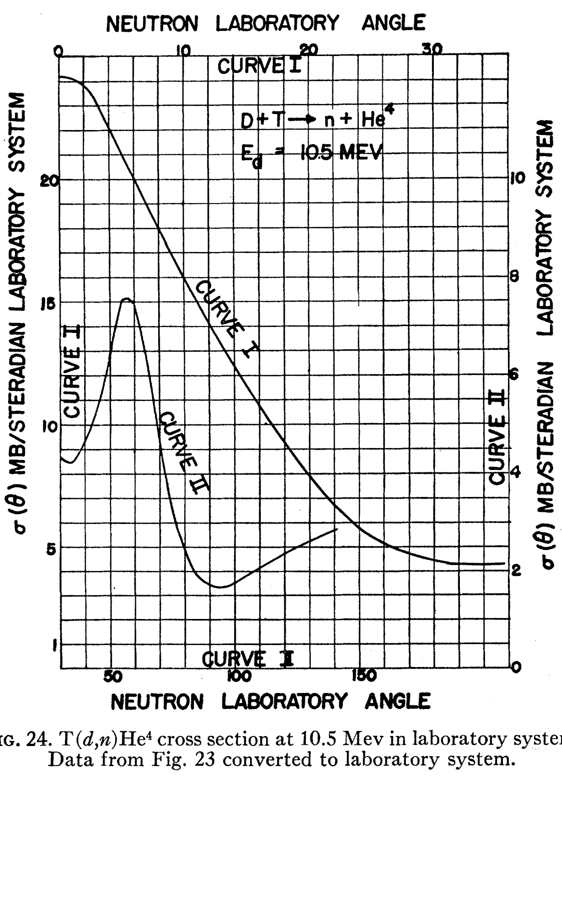

FIG. 24. T(*d*,*n*)He⁴ cross section at 10.5 Mev in laboratory system. Data from Fig. 23 converted to laboratory system.

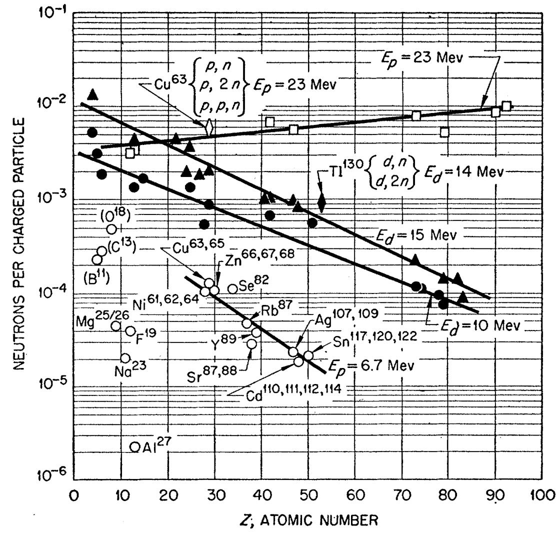

FIG. 25. Thick target yield. For proton and deuteron bombardments as a function of the atomic number of the target material. Proton bombardments: Open squares 55C; open diamond 50G; open circles 51B8, 51B9, and 51B10. Deuteron bombardments: Closed triangles 51A4, closed diamond 46C2, and closed circles 51S2.

It is advantageous in planning monoenergetic neutron experiments to be able to estimate the backgrounds to be expected. In this section is collected some of the information available on thick target neutron yields from high energy (>6 Mev) protons and deuterons. While there are large gaps in our knowledge, there are perhaps sufficient data to enable one to predict the order of magnitude of the backgrounds to be anticipated from materials which limit and stop the bombarding particles.

Figure 25 shows a collection of thick target yields expressed as neutrons per charged particle (protons or deuterons) and plotted as a function of target atomic number at several energies above 6 Mev. The thick target (*p*,*n*) yields at 6.7 Mev were calculated from cross sections *vs* energy curves (51B8, 51B9, 51B10) measured by radioactive product techniques. The data are plotted as if the element consisted of the isotope for which the cross sections are given; in the cases where data are given for more than one isotope per element, the yield is calculated for a mixture of these isotopes in the same relative abundance as they occur in the natural element. The isotopes for which the cross sections are measured are indicated beside the data points. In using these data one is making the assumption that the (*p*,*n*) yields for isotopes for which the (*p*,*n*) cross sections are not given, are about the same as for cases where they are given. The trend of (*p*,*n*) cross sections as a function of atomic number at 6.7 Mev (Fig. 2 of

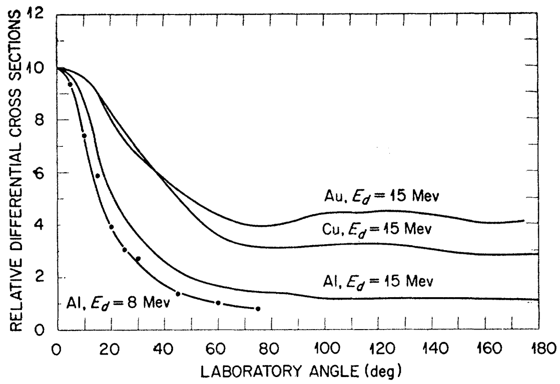

FIG. 26. Relative angular distribution of neutrons from deuteron bombardments of thick targets of Au, Cu, and Al. The 15-Mev deuteron curves, 51A4, 8-Mev bombardment, 51H.

51B9) suggests this is a reasonable assumption. For 23-Mev protons the relative thick target yields were found with an energy insensitive neutron counter (55C) and normalized to the yield calculated from the cross section of Cu for the principle neutron producing reactions (50G). The authors' estimates of the errors of the (p,n) cross sections range for the most part from 10 to 30%.

By means of threshold detectors, $Al^{27}+n\rightarrow Mg^{27}+p-2$ Mev and $Ag^{107}+n\rightarrow Ag^{106}+2n-9.6$ Mev, the angular distributions of higher energy neutrons produced by 23-Mev protons on Mg, Al, Cu, Mo, Ag, Ta, Au, Th, and U were found to be anisotropic. For the Al detector the ratio of the intensity at 0° to that at 180° varied from 1.3 to 5; for the Ag detector this ratio varied from 3 to 15 (55C).

In order to minimize neutron background, one can be guided by two principles in choosing the material which the lower energy proton beams strike. Either one uses a material which has a high (p,n) threshold (C^{12}, for example, has this threshold at $\sim$20 Mev). or one uses a material of high Z so that the reaction rate is cut down by Coulomb effects. Because of the high (p,n) threshold and low cross section, the background from Al is depressed by about two orders of magnitude at 6.7 Mev. At 23 Mev the protons are so much above the Coulomb barrier even for the heaviest

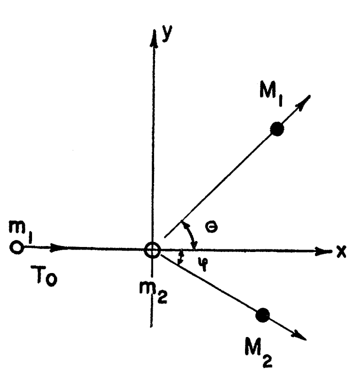

FIG. 27. Laboratory system representation of two particle nuclear reaction with the emission of two different particles.

elements that this barrier effect is not operative; the yield increases slightly with Z.

For deuterons in the 10- to 20-Mev region two sets of thick target yield data are presented. At 10 Mev the number of neutrons was determined by the manganese bath technique; a RaBe source furnished the absolute calibration (51S2). The estimated errors range from about 7 to 30% (averaging 15%). At 15 Mev the neutron intensity was measured with activation detectors (51A4). Most of the measurements were made with sulfur detectors, $S^{32}(n,p)P^{32}$, although the results were checked with phosphorous detectors, $P^{31}(n,p)Si^{32}$, and with fission ionization chambers. The 15-Mev curve, plotted in Fig. 24, has been renormalized to recent measurements with an approximate correction applied to account for neutrons below the detector threshold (55A1). While the relative errors of these 15-Mev data are of the order of magnitude of 10%, there is considerable uncertainty in the absolute normalization (perhaps 50%). The point at $Z=52$ (Te^{130}) was calculated from the $Te^{130}(d,2n)$ and $Te^{130}(d,n)$ yields at 14 Mev

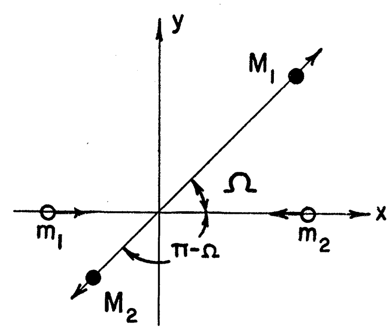

FIG. 28. Center-of-mass system representation of two particle nuclear reaction with the emission of two different particles.

which were measured by radio-chemical analysis of the reaction products (46C2).

Because of the interest in the deuteron stripping phenomena, a number of investigators have measured relative angular distributions of neutrons produced by deuteron bombardments. In Fig. 26 representative angular distributions in the laboratory system are collected for deuteron bombarding energies of 8 and 15 Mev. The 15-Mev data (51A4) were obtained from published curves which omitted experimental points. Comparison of points on either side of 0°, however, suggests that the reproducibility of this data is about 3%. Many of the published results on neutron angular distribution are presented in terms of angular width at 1/2 maximum. Table I summarizes this type of information. In using this table to estimate background one should take into account the energy threshold and response of the detector with which the data are obtained.

The neutron energy spectra produced by high-energy charged particle bombardments ($\sim$10 Mev) for the most part appear to be given approximately by the expression from the statistical theory of nuclear reactions (52B5) for the evaporation of neutrons from a highly excited nucleus; $n(E)\sim E\exp(-E/T)$, where $n(E)$ is the number of neutrons per unit energy interval, E is the neutron energy, and T is a quantity called "nuclear temperature," which, theoretically, is related to the properties of the residual nucleus which has emitted the neutron. T has been found empirically to be of the order of magnitude of 1 Mev. For 16-Mev proton bombardment of 1-Mev thick targets of Al, Fe, Rh, Au, Tl, the spectra at about 0° are found to follow the evaporation expression with the experimental effective nuclear temperatures given in Table II (51C2).

The neutron spectrum at 90° from a thin Cu target bombarded with 10-Mev deuterons shows fluctuations but can be fitted approximately by the evaporation expression with a nuclear temperature of about 1.1 Mev (49G2). At 15-Mev deuteron bombardment energy the neutron spectra are represented approximately by the evaporation expression, but the effective nuclear temperatures depend on the angle to the beam direction (51C3). Because of the phenomena of deuteron stripping, the spectra at small angles are expected to differ from those at larger angles where compound nucleus phenomena are expected to be more important. Table II gives a summary of the neutron spectra observed for high energy charged particle bombardment of elements above $Z=12$. The experimental nuclear temperatures quoted are estimated from the mean slope of the experimental curves.

CONCLUSION

Experimental neutron physics in the energy region we have been discussing has made considerable progress in the last decade. Advancement of the field however has been principally in the refinement of techniques rather than the introduction of new concepts. The present state of precision in the field leaves much to be desired.

TABLE I. Angular width at ½ intensity for neutron distributions from (d,n) reactions.

Detector	Biased counter	$S^{32}(n,p)$	Neutron telescope	$Ag^{107}(n,2n)$	$Cu^{63}(n,2n)$	$Cu^{63}(n,2n)$
Threshold (Mev)	~1.5	0.97	9.30–13.1	5–7	11	11
Reference	51H	51A4	51F2	49F	49F	49A
E_d(Mev)	8	15	15	16	16	18
Element						
Al	17°	21°	12°			
Si	15°					
S	20°					
Ti		39°	20°			
Cr		36°				
Mn		37°				
Co		39°	22°		26°	
Cu		46°	22½°	48°	26°	45°
Cb		46°				
Mo		42°	25°			
Ag			21°			
Cd		51°				
Ta		57°				
Au		52°	23°	49°		
Pb		51°				47°
Bi		58°				

TABLE II. Nuclear temperatures for neutron evaporation.

Bombarding particle	Protons	Deuterons		
Angle to beam	~0°	90°	0°	90°
Target	thin	thin	thick	thick
Reference	51G	49G2	51C2	51C2
E(Mev)	16	10	15	15
Element				
Al	1.30		2.0	2.0
Fe	0.95			
Co			2.5	1.7
Cu		1.1	2.5	1.7
Rh	0.85			
Au	0.80			
Tl	0.78			

ACKNOWLEDGMENTS

We wish to thank our many colleagues for their contributions.

APPENDIX I

For the light particle reactions which lead to the production of monoenergetic neutrons, the conversion of laboratory cross sections and angles to the c.m. system is generally done in the nonrelativistic approximation. The following relationships (see Figs. 27 and 28) are condensed from a report by Carlson, Goldstein, Rosen, and Sweeney (49C3).

Let

m_1 = mass of the incident particle,

E_0 = energy of the incident particle,

m_2 = mass of the bombarded particle,

M_1 = mass of the lighter product nucleus,

M_2 = mass of the heavier product nucleus,

Q = reaction energy,

$$E_T=E_0+Q.$$

Then if

Ω = c.m. angle

θ = laboratory angle of M_1,

ϕ = laboratory angle of M_2,

E_1 = laboratory energy of M_1,

E_2 = laboratory energy of M_2,

$$A_1=\frac{m_1M_2}{(M_1+M_2)^2}(1-Q/E_T),$$

$$B_1=\frac{m_2M_1}{(M_1+M_2)^2}\left(\frac{M_1+M_2-m_1}{m_2}+\frac{m_1}{m_2}\frac{Q}{E_T}\right),$$

$$A_2=\frac{m_1M_1}{(M_1+M_2)^2}\left(1-\frac{Q}{E_T}\right),$$

$$B_2=\frac{m_2M_2}{(M_1+M_2)^2}\left(\frac{M_1+M_2-m_1}{m_2}+\frac{m_1}{m_2}\frac{Q}{E_T}\right).$$

The following useful relations may be obtained:

$$\sin\phi=\left(\frac{B_1}{E_2/E_T}\right)^{\frac{1}{2}}\sin\Omega,$$

$$\sin\theta=\left(\frac{B_2}{E_1/E_T}\right)^{\frac{1}{2}}\sin\Omega,$$

$$\sin\phi=\left(\frac{M_1}{M_2}\frac{E_1/E_T}{A_1+B_1+A_2+B_2-E_1/E_T}\right)^{\frac{1}{2}}\sin\theta,$$

$$\frac{E_2}{E_T}=A_1\left[\cos\phi\pm\left(\frac{B_1}{A_1}-\sin^2\phi\right)^{\frac{1}{2}}\right]^2,\dagger\dagger$$

$$\frac{E_1}{E_T}=A_2\left[\cos\theta\pm\left(\frac{B_2}{A_2}-\sin^2\theta\right)^{\frac{1}{2}}\right]^2.\ddagger\ddagger$$

The cross sections will transform as

$$\frac{\sigma(\Omega)}{\sigma(\phi)}=\frac{(A_1B_1)^{\frac{1}{2}}\left(\frac{B_1}{A_1}-\sin^2\phi\right)^{\frac{1}{2}}}{E_2/E_T}$$

$$\frac{\sigma(\Omega)}{\sigma(\theta)}=\frac{(A_1B_1)^{\frac{1}{2}}\left(\frac{B_2}{A_2}-\sin^2\theta\right)^{\frac{1}{2}}}{E_1/E_T}.$$

APPENDIX II

The precision of the energy of accelerators has reached the stage that for some purposes one should use the correct relativistic equations to find the energy of neutrons produced by nuclear reactions. Since these relativistic transformations are very tedious there is a growing need for computed tables for this purpose. In this appendix are collected such tables of neutron energies as a function of laboratory angle and bombarding energies for the $T(p,n)He^3$, the $D(d,n)He^3$, and the $T(d,n)He^4$ reactions. These tables are taken from a more complete set which included relativistic transformations of center-of-mass angle to the laboratory angle and the ratio of solid angles in the two systems for both neutron and the helium nuclei produced in the reactions. The tables were calculated by L. Blumberg and S. I. Schlesinger and are to be printed as a Los Alamos document (55B2).

The expressions used in the formulation of Tables III, IV, and V may be derived from the relativistic kinematics of the two-body reaction problem. Consider, as in Fig. 27, that a particle of rest mass m_1 and kinetic energy T_0 is incident along the x-axis on a target particle of rest mass m_2 at rest in the laboratory system. The reaction products with rest masses M_1 and M_2 emerge at angles θ and ϕ respectively with the x-axis. In the c.m. system, the collision appears as in Fig. 28.

The total energy of the reaction products may be obtained from a Lorentz transformation of the components of the momentum four vector $\mathbf{P}(p_x, p_y, p_z, E/c^2)$ as

$$E_n(\theta)=M_nc^2[\gamma_n\gamma_{cg}\pm(\gamma_{cg}^2-1)^{\frac{1}{2}}(\gamma_n^2-1)^{\frac{1}{2}}\cos\Omega]; \quad n=1,2 \tag{1}$$

where the plus sign is associated with the subscript $n=1$, the negative sign with subscript $n=2$, and where the $\cos\Omega$ is obtained from the transformation of p_x and p_y as

$$\cos\Omega=\frac{-\alpha_1\gamma_{cg}^2\tan^2\theta\pm[1-(\alpha_1^2-1)\gamma_{cg}^2\tan^2\theta]^{\frac{1}{2}}}{1+\gamma_{cg}^2\tan^2\theta} \tag{2}$$

where

$$\alpha_1=\frac{\gamma_1(\gamma_{cg}^2-1)^{\frac{1}{2}}}{\gamma_{cg}(\gamma_1^2-1)^{\frac{1}{2}}}.$$

An expression for γ_{cg} is derived from the transformation of P_{x1} to the c.m. system as

$$\gamma_{cg}=\frac{\frac{m_2}{m_1}+\gamma_0}{\left[\left(\frac{m_2}{m_1}\right)^2+2\left(\frac{m_2}{m_1}\right)\gamma_0+1\right]^{\frac{1}{2}}} \tag{3}$$

where $\gamma_0=(T_0/m_1c^2)+1$. After the reaction has occurred, the conservation of energy in the c.m. system yields the relation for γ_n as

$$\gamma_n=\frac{(m_1^2+2m_1m_2\gamma_0+m_2^2)\pm(M_1^2-M_2^2)}{2M_n(m_1^2+2m_1m_2\gamma_0+m_2^2)^{\frac{1}{2}}}; \quad n=1,2 \tag{4}$$

where again the positive and negative signs are associated with $n=1$, 2, respectively.

Inspection of Eq. (2) reveals that there are three possible cases, namely $\alpha_1\gtreqless 1$.

Case A: ($\alpha_1>1$)

To define $\cos\Omega$ in the interval $0\leq\Omega\leq\pi$, both the positive and negative radical must be used and consequently $\cos\Omega$ is double valued. The maximum value of θ occurs when the radical is zero and is given by

$$\theta_{\max}=\sin^{-1}\{[1+\gamma_{cg}^2(\alpha_1^2-1)]^{-\frac{1}{2}}\} \tag{5}$$

where $\theta_{\max}<\pi/2$.

Case B: ($\alpha_1<1$)

$\cos\Omega$ is defined for all values $0\leq\theta\leq\pi$ with the stipulation that the positive sign is used for $\theta<\pi/2$ and the negative sign for $\theta>\pi/2$. Hence $\cos\Omega$ is single valued.

†† Use both signs if $A_1>B_1$, in which case $\phi_{\max}=\arcsin(B_2/A_2)^{\frac{1}{2}}$. Use only the plus sign if $A_1\leq B_1$.

‡‡ Use both signs if $A_2>B_2$, in which case $\theta_{\max}=\arcsin(B_1/A_1)^{\frac{1}{2}}$. Use only the plus sign if $A_2\leq B_2$.

TABLE III

T + p ⟶ He³ + n Reaction

3.0170050 + 1.0081450 ⟶ 3.0169860 + 1.0089861

θ	Proton Energy											
	1.1000	1.2000	1.3000	1.4000	1.5000	1.6000	1.7000	1.8000	1.9000	2.0000	2.1000	2.2000
0	0.2238	0.3497	0.4643	0.5741	0.6814	0.7869	0.8914	0.9951	1.0982	1.2008	1.3030	1.4050
5	0.2217	0.3474	0.4617	0.5713	0.6783	0.7836	0.8878	0.9912	1.0941	1.1964	1.2983	1.4001
10	0.2154	0.3406	0.4542	0.5630	0.6692	0.7737	0.8772	0.9798	1.0818	1.1835	1.2846	1.3856
15	0.2051	0.3294	0.4418	0.5493	0.6543	0.7575	0.8597	0.9610	1.0618	1.1622	1.2620	1.3617
20	0.1910	0.3143	0.4250	0.5308	0.6339	0.7354	0.8358	0.9354	1.0344	1.1330	1.2312	1.3291
30	0.1535	0.2739	0.3799	0.4809	0.5792	0.6759	0.7715	0.8663	0.9605	1.0543	1.1477	1.2409
40	0.1067	0.2242	0.3241	0.4188	0.5107	0.6010	0.6903	0.7789	0.8668	0.9545	1.0417	1.1287
50	0.0528	0.1710	0.2634	0.3504	0.4348	0.5177	0.5997	0.6809	0.7616	0.8421	0.9221	1.0020
60		0.1203	0.2039	0.2823	0.3584	0.4331	0.5070	0.5804	0.6533	0.7259	0.7982	0.8704
70		0.0773	0.1508	0.2199	0.2871	0.3534	0.4190	0.4843	0.5492	0.6139	0.6784	0.7427
80		0.0454	0.1074	0.1669	0.2252	0.2831	0.3406	0.3979	0.4550	0.5120	0.5689	0.6257
90		0.0251	0.0749	0.1248	0.1746	0.2245	0.2744	0.3243	0.3740	0.4240	0.4738	0.5236
100		0.0139	0.0522	0.0934	0.1354	0.1781	0.2210	0.2642	0.3075	0.3511	0.3946	0.4382
110		0.0082	0.0372	0.0708	0.1062	0.1427	0.1796	0.2171	0.2548	0.2928	0.3309	0.3691
120		0.0053	0.0275	0.0552	0.0851	0.1164	0.1485	0.1812	0.2142	0.2476	0.2812	0.3150
130		0.0037	0.0213	0.0445	0.0702	0.0974	0.1256	0.1544	0.1837	0.2135	0.2435	0.2737
140		0.0028	0.0173	0.0372	0.0597	0.0839	0.1091	0.1350	0.1614	0.1884	0.2155	0.2429
150		0.0023	0.0148	0.0324	0.0527	0.0746	0.0976	0.1214	0.1457	0.1705	0.1956	0.2210
160		0.0020	0.0132	0.0294	0.0481	0.0686	0.0901	0.1124	0.1353	0.1587	0.1824	0.2063
170		0.0019	0.0124	0.0277	0.0456	0.0652	0.0859	0.1073	0.1294	0.1519	0.1748	0.1979
180		0.0018	0.0121	0.0272	0.0448	0.0641	0.0845	0.1057	0.1274	0.1497	0.1723	0.1952

θ	2.3000	2.4000	2.5000	2.6000	2.7000	2.8000	2.9000	3.0000	3.1000	3.2000	3.3000	3.4000
0	1.5067	1.6082	1.7096	1.8109	1.9119	2.0131	2.1139	2.2148	2.3155	2.4164	2.5169	2.6177
5	1.5015	1.6028	1.7039	1.8050	1.9058	2.0066	2.1072	2.2079	2.3083	2.4089	2.5092	2.6097
10	1.4862	1.5868	1.6871	1.7874	1.8874	1.9875	2.0873	2.1872	2.2869	2.3867	2.4863	2.5860
15	1.4611	1.5604	1.6595	1.7585	1.8573	1.9561	2.0547	2.1533	2.2517	2.3503	2.4486	2.5470
20	1.4268	1.5243	1.6217	1.7190	1.8160	1.9131	2.0100	2.1068	2.2036	2.3004	2.3970	2.4937
30	1.3339	1.4266	1.5193	1.6118	1.7041	1.7965	1.8886	1.9808	2.0728	2.1649	2.2568	2.3488
40	1.2155	1.3022	1.3887	1.4751	1.5613	1.6475	1.7336	1.8196	1.9056	1.9916	2.0774	2.1633
50	1.0817	1.1612	1.2406	1.3199	1.3991	1.4783	1.5573	1.6363	1.7152	1.7942	1.8730	1.9518
60	0.9425	1.0143	1.0861	1.1578	1.2295	1.3011	1.3725	1.4440	1.5154	1.5868	1.6581	1.7295
70	0.8070	0.8712	0.9353	0.9993	1.0633	1.1273	1.1911	1.2549	1.3188	1.3826	1.4463	1.5101
80	0.6825	0.7392	0.7959	0.8526	0.9092	0.9658	1.0223	1.0789	1.1354	1.1920	1.2484	1.3050
90	0.5735	0.6233	0.6732	0.7230	0.7728	0.8227	0.8725	0.9223	0.9721	1.0219	1.0717	1.1216
100	0.4819	0.5255	0.5693	0.6131	0.6569	0.7007	0.7446	0.7884	0.8323	0.8762	0.9201	0.9640
110	0.4075	0.4459	0.4845	0.5231	0.5617	0.6004	0.6391	0.6778	0.7166	0.7554	0.7942	0.8331
120	0.3490	0.3830	0.4172	0.4515	0.4858	0.5202	0.5546	0.5891	0.6237	0.6582	0.6928	0.7274
130	0.3041	0.3346	0.3653	0.3961	0.4269	0.4579	0.4889	0.5199	0.5510	0.5822	0.6134	0.6446
140	0.2706	0.2984	0.3264	0.3544	0.3826	0.4109	0.4392	0.4676	0.4960	0.5245	0.5531	0.5816
150	0.2466	0.2724	0.2983	0.3244	0.3506	0.3768	0.4032	0.4296	0.4560	0.4826	0.5091	0.5358
160	0.2306	0.2549	0.2795	0.3042	0.3290	0.3539	0.3788	0.4039	0.4290	0.4542	0.4794	0.5047
170	0.2214	0.2449	0.2687	0.2925	0.3165	0.3406	0.3648	0.3891	0.4134	0.4378	0.4622	0.4867
180	0.2184	0.2416	0.2651	0.2887	0.3125	0.3363	0.3602	0.3842	0.4083	0.4324	0.4566	0.4808

θ	3.5000	3.6000	3.7000	3.8000	3.9000	4.0000	4.1000	4.2000	4.3000	4.4000	4.5000	4.6000
0	2.7181	2.8188	2.9192	3.0198	3.1201	3.2206	3.3209	3.4214	3.5216	3.6220	3.7223	3.8227
5	2.7099	2.8103	2.9105	3.0108	3.1109	3.2111	3.3112	3.4114	3.5114	3.6115	3.7115	3.8117
10	2.6854	2.7850	2.8845	2.9840	3.0833	3.1828	3.2821	3.3816	3.4808	3.5802	3.6794	3.7788
15	2.6452	2.7436	2.8418	2.9400	3.0381	3.1363	3.2344	3.3326	3.4305	3.5287	3.6266	3.7248
20	2.5902	2.6868	2.7833	2.8798	2.9762	3.0727	3.1690	3.2655	3.3617	3.4581	3.5544	3.6508
30	2.4406	2.5325	2.6243	2.7161	2.8078	2.8996	2.9912	3.0830	3.1745	3.2662	3.3578	3.4495
40	2.2491	2.3349	2.4206	2.5063	2.5920	2.6777	2.7632	2.8489	2.9344	3.0201	3.1056	3.1912
50	2.0306	2.1093	2.1881	2.2668	2.3454	2.4241	2.5027	2.5814	2.6599	2.7385	2.8170	2.8957
60	1.8007	1.8720	1.9432	2.0144	2.0856	2.1568	2.2279	2.2991	2.3702	2.4413	2.5124	2.5835
70	1.5738	1.6375	1.7012	1.7649	1.8285	1.8922	1.9558	2.0194	2.0830	2.1466	2.2102	2.2738
80	1.3614	1.4179	1.4743	1.5308	1.5872	1.6436	1.7000	1.7565	1.8128	1.8692	1.9256	1.9820
90	1.1714	1.2212	1.2710	1.3208	1.3706	1.4204	1.4702	1.5200	1.5698	1.6195	1.6693	1.7191
100	1.0079	1.0518	1.0957	1.1397	1.1836	1.2275	1.2714	1.3154	1.3593	1.4032	1.4472	1.4912
110	0.8719	0.9108	0.9497	0.9885	1.0274	1.0663	1.1052	1.1442	1.1831	1.2220	1.2609	1.2999
120	0.7621	0.7967	0.8315	0.8661	0.9008	0.9356	0.9703	1.0051	1.0398	1.0746	1.1094	1.1441
130	0.6759	0.7071	0.7385	0.7698	0.8011	0.8325	0.8638	0.8952	0.9266	0.9580	0.9895	1.0209
140	0.6103	0.6389	0.6676	0.6963	0.7250	0.7537	0.7825	0.8113	0.8400	0.8688	0.8976	0.9265
150	0.5624	0.5891	0.6158	0.6426	0.6693	0.6961	0.7229	0.7497	0.7766	0.8034	0.8303	0.8572
160	0.5300	0.5553	0.5807	0.6061	0.6315	0.6569	0.6824	0.7079	0.7334	0.7589	0.7844	0.8100
170	0.5112	0.5357	0.5603	0.5849	0.6096	0.6342	0.6589	0.6836	0.7083	0.7330	0.7578	0.7826
180	0.5051	0.5293	0.5537	0.5780	0.6024	0.6268	0.6512	0.6757	0.7001	0.7246	0.7491	0.7736

TABLE III (continued)

θ	Proton Energy											
	4.7000	4.8000	4.9000	5.0000	5.1000	5.2000	5.3000	5.4000	5.5000	5.6000	5.7000	5.8000
0	3.9229	4.0233	4.1234	4.2237	4.3240	4.4242	4.5245	4.6246	4.7248	4.8249	4.9252	5.0254
5	3.9116	4.0117	4.1116	4.2116	4.3117	4.4116	4.5116	4.6115	4.7115	4.8114	4.9113	5.0113
10	3.8780	3.9773	4.0765	4.1757	4.2750	4.3741	4.4734	4.5725	4.6718	4.7709	4.8701	4.9693
15	3.8227	3.9208	4.0187	4.1167	4.2147	4.3126	4.4106	4.5085	4.6065	4.7043	4.8023	4.9002
20	3.7470	3.8434	3.9396	4.0358	4.1321	4.2283	4.3246	4.4207	4.5170	4.6131	4.7094	4.8056
30	3.5410	3.6327	3.7242	3.8157	3.9074	3.9988	4.0904	4.1819	4.2734	4.3649	4.4564	4.5479
40	3.2767	3.3623	3.4477	3.5332	3.6188	3.7042	3.7897	3.8751	3.9606	4.0460	4.1315	4.2169
50	2.9742	3.0528	3.1312	3.2097	3.2883	3.3667	3.4453	3.5237	3.6022	3.6806	3.7591	3.8375
60	2.6546	2.7257	2.7967	3.8677	2.9388	3.0098	3.0808	3.1518	3.2229	3.2938	3.3648	3.4358
70	2.3373	2.4009	2.4645	2.5280	2.5915	2.6550	2.7186	2.7821	2.8456	2.9091	2.9726	3.0361
80	2.0384	2.0948	2.1512	2.2075	2.2638	2.3202	2.3766	2.4329	2.4892	2.5456	2.6019	2.6582
90	1.7689	1.8187	1.8685	1.9182	1.9680	2.0178	2.0675	2.1173	2.1670	2.2168	2.2665	2.3163
100	1.5351	1.5790	1.6230	1.6669	1.7108	1.7548	1.7987	1.8427	1.8866	1.9305	1.9745	2.0184
110	1.3389	1.3778	1.4168	1.4556	1.4946	1.5336	1.5725	1.6115	1.6504	1.6894	1.7283	1.7673
120	1.1790	1.2137	1.2486	1.2833	1.3181	1.3529	1.3877	1.4226	1.4574	1.4922	1.5270	1.5618
130	1.0524	1.0838	1.1153	1.1467	1.1781	1.2096	1.2411	1.2726	1.3041	1.3356	1.3670	1.3985
140	0.9553	0.9841	1.0130	1.0418	1.0707	1.0996	1.1284	1.1573	1.1862	1.2151	1.2440	1.2729
150	0.8841	0.9110	0.9379	0.9648	0.9917	1.0187	1.0456	1.0726	1.0995	1.1265	1.1534	1.1804
160	0.8356	0.8611	0.8867	0.9123	0.9378	0.9635	0.9891	1.0147	1.0403	1.0660	1.0916	1.1172
170	0.8074	0.8322	0.8570	0.8817	0.9066	0.9314	0.9562	0.9811	1.0059	1.0308	1.0556	1.0805
180	0.7982	0.8227	0.8472	0.8717	0.8963	0.9209	0.9455	0.9701	0.9946	1.0193	1.0438	1.0684
	5.9000	6.0000	6.1000	6.2000	6.3000	6.4000	6.5000	6.6000	6.8000	7.0000	7.2000	7.4000
0	5.1255	5.2257	5.3258	5.4260	5.5262	5.6263	5.7265	5.8265	6.0269	6.2271	6.4273	6.6275
5	5.1111	5.2111	5.3109	5.4109	5.5108	5.6107	5.7106	5.8104	6.0103	6.2099	6.4096	6.6093
10	5.0684	5.1676	5.2666	5.3658	5.4650	5.5640	5.6633	5.7623	5.9606	6.1587	6.3569	6.5550
15	4.9980	5.0960	5.1938	5.2917	5.3897	5.4875	5.5854	5.6832	5.8790	6.0746	6.2703	6.4659
20	4.9017	4.9979	5.0940	5.1902	5.2864	5.3825	5.4787	5.5748	5.7671	5.9593	6.1515	6.3437
30	4.6394	4.7309	4.8223	4.9138	5.0053	5.0967	5.1882	5.2796	5.4625	5.6453	5.8281	6.0109
40	4.3023	4.3878	4.4731	4.5586	4.6440	4.7294	4.8148	4.9001	5.0709	5.2416	5.4123	5.5830
50	3.9159	3.9944	4.0728	4.1512	4.2297	4.3080	4.3865	4.4648	4.6217	4.7784	4.9351	5.0918
60	3.5068	3.5778	3.6487	3.7197	3.7907	3.8616	3.9326	4.0035	4.1454	4.2873	4.4291	4.5709
70	3.0096	3.1631	3.2265	3.2900	3.3535	3.4170	3.4805	3.5439	3.6708	3.7977	3.9245	4.0514
80	2.7145	2.7708	2.8272	2.8835	2.9398	2.9961	3.0524	3.1087	3.2213	3.3338	3.4464	3.5589
90	2.3660	2.4158	2.4655	2.5152	2.5650	2.6147	2.6645	2.7142	2.8136	2.9131	3.0125	3.1119
100	2.0623	2.1062	2.1502	2.1941	2.2380	2.2820	2.3259	2.3698	2.4577	2.5455	2.6333	2.7212
110	1.8063	1.8452	1.8842	1.9231	1.9621	2.0010	2.0400	2.0790	2.1569	2.2348	2.3127	2.3906
120	1.5967	1.6315	1.6663	1.7011	1.7360	1.7708	1.8057	1.8405	1.9101	1.9798	2.0495	2.1191
130	1.4300	1.4615	1.4931	1.5245	1.5560	1.5876	1.6191	1.6506	1.7136	1.7766	1.8396	1.9027
140	1.3018	1.3307	1.3596	1.3885	1.4174	1.4463	1.4753	1.5042	1.5620	1.6199	1.6777	1.7356
150	1.2074	1.2343	1.2613	1.2883	1.3153	1.3423	1.3693	1.3963	1.4502	1.5042	1.5583	1.6123
160	1.1429	1.1685	1.1942	1.2198	1.2455	1.2712	1.2968	1.3225	1.3738	1.4252	1.4765	1.5279
170	1.1054	1.1302	1.1551	1.1800	1.2048	1.2298	1.2547	1.2796	1.3293	1.3791	1.4[illegible]99	1.4788
180	1.0931	1.1177	1.1423	1.1669	1.1915	1.2162	1.2408	1.2655	1.3147	1.3640	1.4133	1.4626
	7.6000	7.8000	8.0000	8.5000	9.0000	9.5000	10.0000	10.5000	11.0000	11.5000	12.0000	12.5000
0	6.8278	7.0279	7.2281	7.7286	8.2288	8.7292	9.2295	9.7297	10.2300	10.7303	11.2305	11.7306
5	6.8091	7.0087	7.2083	7.7076	8.2065	8.7056	9.2046	9.7036	10.2026	10.7015	11.2004	11.6993
10	6.7533	6.9514	7.1495	7.6449	8.1401	8.6353	9.1305	9.6256	10.1208	10.6159	11.1110	11.6060
15	6.6617	6.8572	7.0528	7.5420	8.0308	8.5198	9.0086	9.4975	9.9864	10.4752	10.9640	11.4527
20	6.5360	6.7282	6.9203	7.4009	7.8811	8.3614	8.8417	9.3219	9.8021	10.2823	10.7625	11.2425
30	6.1938	6.3766	6.5593	7.0163	7.4731	7.9299	8.3866	8.8433	9.3000	9.7566	10.2131	10.6696
40	5.7538	5.9244	6.0950	6.5217	6.9481	7.3746	7.8010	8.2273	8.6536	9.0799	9.5060	9.9321
50	5.2486	4.4053	5.5619	5.9537	6.3451	6.7367	7.1281	7.5194	7.9108	8.3020	8.6932	9.0843
60	4.7128	4.8545	4.9963	5.3508	5.7050	6.0592	6.4134	6.7675	7.1215	7.4754	7.8293	8.1831
70	4.1782	4.3050	4.4318	4.7489	5.0657	5.3825	5.6993	6.0159	6.3325	6.6490	6.9655	7.2818
80	3.6715	3.7839	3.8964	4.1777	4.4588	4.7398	5.0208	5.3017	5.5825	5.8633	6.1440	6.4246
90	3.2113	3.3107	3.4101	3.6586	3.9069	4.1551	4.4034	4.6515	4.8996	5.1476	5.3956	5.6434
100	2.8090	2.8967	2.9846	3.2040	3.4234	3.6427	3.8621	4.0813	4.3004	4.5195	4.7386	4.9575
110	2.4685	2.5463	2.6242	2.8189	3.0135	3.2081	3.4027	3.5972	3.7916	3.9860	4.1803	4.3745
120	2.1888	2.2584	2.3281	2.5022	2.6763	2.8503	3.0244	3.1983	3.3722	3.5461	3.7199	3.8936
130	1.9657	2.0287	2.0917	2.2493	2.4067	2.5642	2.7217	2.8791	3.0365	3.1938	3.3511	3.5083
140	1.7934	1.8512	1.9091	2.0537	2.1983	2.3429	2.4875	2.6320	2.7765	2.9210	3.0654	3.2098
150	1.6663	1.7203	1.7743	1.9093	2.0443	2.1793	2.3143	2.4493	2.5842	2.7191	2.8539	2.9887
160	1.5792	1.6306	1.6820	1.8104	1.9388	2.0672	2.1956	2.3239	2.4523	2.5806	2.7088	2.8370
170	1.5286	1.5784	1.6282	1.7528	1.8773	2.0018	2.1264	2.2509	2.3754	2.4998	2.6242	2.7486
180	1.5119	1.5612	1.6106	1.7339	1.8571	1.9804	2.1037	2.2269	2.3501	2.4733	2.5964	2.7195

TABLE III (continued)

θ	Proton Energy											
	13.0000	13.5000	14.0000	14.5000	15.0000	16.0000	17.0000	18.0000	19.0000	20.0000	21.0000	22.0000
0	12.2307	12.7309	13.2311	13.7312	14.2312	15.2316	16.2316	17.2319	18.2320	19.2322	20.2322	21.2323
5	12.1981	12.6970	13.1959	13.6947	14.1934	15.1912	16.1887	17.1863	18.1839	19.1815	20.1789	21.1764
10	12.1010	12.5960	13.0911	13.5861	14.0810	15.0710	16.0608	17.0507	18.0406	19.0304	20.0202	21.0099
15	11.9414	12.4301	12.9189	13.4075	13.8961	14.8735	15.8506	16.8279	17.8050	18.7822	19.7592	20.7362
20	11.7225	12.2026	12.6827	13.1627	13.6426	14.6027	15.5624	16.5223	17.4821	18.4418	19.4014	20.3610
30	11.1261	11.5825	12.0390	12.4954	12.9517	13.8644	14.7769	15.6894	16.6017	17.5140	18.4260	19.3381
40	10.3582	10.7842	11.2102	11.6362	12.0620	12.9138	13.7653	14.6168	15.4680	16.3191	17.1701	18.0209
50	9.4753	9.8664	10.2573	10.6482	11.0390	11.8206	12.6019	13.3831	14.1641	14.9449	15.7254	16.5059
60	8.5368	8.8906	9.2442	9.5978	9.9512	10.6581	11.3647	12.0711	12.7773	13.4832	14.1888	14.8943
70	7.5981	7.9144	8.2306	8.5467	8.8627	9.4947	10.1263	10.7577	11.3889	12.0198	12.6504	13.2808
80	6.7051	6.9857	7.2661	7.5465	7.8267	8.3871	8.9472	9.5071	10.0667	10.6261	11.1851	11.7439
90	5.8912	6.1391	6.3867	6.6344	6.8819	7.3768	7.8715	8.3659	8.8600	9.3539	9.8475	10.3408
100	5.1764	5.3953	5.6141	5.8329	6.0515	6.4886	6.9255	7.3622	7.7986	8.2347	8.6706	9.1062
110	4.5688	4.7630	4.9570	5.1511	5.3451	5.7328	6.1204	6.5077	6.8948	7.2816	7.6681	8.0545
120	4.0673	4.2410	4.4146	4.5882	4.7617	5.1085	5.4551	5.8015	6.1477	6.4936	6.8392	7.1847
130	3.6655	3.8227	3.9798	4.1369	4.2939	4.6077	4.9213	5.2348	5.5480	5.8610	6.1738	6.4864
140	3.3541	3.4985	3.6426	3.7869	3.9311	4.2192	4.5072	4.7950	5.0826	5.3700	5.6571	5.9441
150	3.1235	3.2583	3.3929	3.5276	3.6622	3.9313	4.2002	4.4689	4.7375	5.0058	5.2739	5.5419
160	2.9652	3.0935	3.2215	3.3496	3.4777	3.7336	3.9894	4.2450	4.5004	4.7557	5.0107	5.2655
170	2.8729	2.9973	3.1215	3.2458	3.3700	3.6182	3.8664	4.1143	4.3621	4.6096	4.8570	5.1042
180	2.8426	2.9657	3.0887	3.2117	3.3346	3.5803	3.8259	4.0714	4.3166	4.5616	4.8065	5.0512

θ	23.0000	24.0000	25.0000
0	22.2325	23.2326	24.2326
5	22.1740	23.1714	24.1689
10	21.9997	22.9894	23.9791
15	21.7133	22.6902	23.6671
20	21.3206	22.2801	23.2395
30	20.2501	21.1619	22.0737
40	18.8716	19.7221	20.5725
50	17.2861	18.0661	18.8459
60	15.5996	16.3046	17.0094
70	13.9110	14.5409	15.1705
80	12.3025	12.8607	13.4188
90	10.8339	11.3267	11.8193
100	9.5416	9.9767	10.4115
110	8.4406	8.8264	9.2120
120	7.5300	7.8749	8.2197
130	6.7987	7.1108	7.4228
140	6.2309	6.5174	6.8038
150	5.8096	6.0772	6.3445
160	5.5202	5.7746	6.0289
170	5.3512	5.5980	5.8447
180	5.2957	5.5400	5.7841

TABLE IV

D + D ⟶ He^3 + n

2.0147400 + 2.0147400 ⟶ 3.0169860 + 1.0089861

θ	Deuteron Energy											
	0.1000	0.2000	0.3000	0.4000	0.5000	0.6000	0.7000	0.8000	0.9000	1.0000	1.1000	1.2000
0	2.8504	3.0500	3.2177	3.3690	3.5099	3.6438	3.7723	3.8969	4.0182	4.1368	4.2530	4.3675
5	2.8489	3.0477	3.2148	3.3654	3.5057	3.6391	3.7671	3.8912	4.0121	4.1302	4.2459	4.3599
10	2.8443	3.0408	3.2059	3.3548	3.4934	3.6252	3.7517	3.8743	3.9937	4.1104	4.2247	4.3373
15	2.8367	3.0294	3.1912	3.3372	3.4731	3.6023	3.7263	3.8464	3.9634	4.0777	4.1897	4.3001
20	2.8261	3.0135	3.1710	3.3129	3.4451	3.5707	3.6912	3.8080	3.9217	4.0328	4.1416	4.2488
30	2.7966	2.9695	3.1148	3.2456	3.3675	3.4832	3.5943	3.7018	3.8066	3.9089	4.0090	4.1077
40	2.7571	2.9108	3.0400	3.1564	3.2648	3.3677	3.4665	3.5622	3.6553	3.7462	3.8353	3.9231
50	2.7092	2.8400	2.9501	3.0495	3.1422	3.2303	3.3148	3.3967	3.4764	3.5544	3.6307	3.7058
60	2.6546	2.7600	2.8492	2.9301	3.0057	3.0777	3.1469	3.2141	3.2795	3.3435	3.4063	3.4682
70	2.5955	2.6741	2.7415	2.8032	2.8613	2.9169	2.9707	3.0229	3.0741	3.1242	3.1734	3.2221
80	2.5340	2.5854	2.6311	2.6739	2.7149	2.7546	2.7934	2.8314	2.8688	2.9056	2.9421	2.9783
90	2.4721	2.4970	2.5218	2.5467	2.5716	2.5965	2.6214	2.6463	2.6712	2.6960	2.7209	2.7458
100	2.4116	2.4116	2.4171	2.4256	2.4360	2.4475	2.4601	2.4734	2.4872	2.5016	2.5164	2.5315
110	2.3545	2.3316	2.3198	2.3137	2.3113	2.3113	2.3133	2.3167	2.3212	2.3266	2.3330	2.3400
120	2.3021	2.2590	2.2321	2.2135	2.2003	2.1906	2.1838	2.1790	2.1758	2.1741	2.1736	2.1741
130	2.2557	2.1954	2.1558	2.1269	2.1048	2.0872	2.0733	2.0619	2.0527	2.0452	2.0394	2.0347
140	2.2165	2.1420	2.0921	2.0549	2.0258	2.0021	1.9826	1.9662	1.9523	1.9405	1.9306	1.9222
150	2.1852	2.0997	2.0419	1.9984	1.9641	1.9357	1.9122	1.8921	1.8748	1.8599	1.8471	1.8359
160	2.1624	2.0690	2.0057	1.9579	1.9199	1.8883	1.8620	1.8394	1.8198	1.8028	1.7880	1.7750
170	2.1486	2.0505	1.9839	1.9334	1.8933	1.8600	1.8320	1.8079	1.7871	1.7688	1.7529	1.7388
180	2.1440	2.0443	1.9766	1.9253	1.8845	1.8505	1.8220	1.7975	1.7762	1.7575	1.7412	1.7268
	1.3000	1.4000	1.5000	1.6000	1.7000	1.8000	1.9000	2.0000	2.1000	2.2000	2.3000	2.4000
0	4.4804	4.5916	4.7018	4.8107	4.9188	5.0259	5.1321	5.2378	5.3427	5.4471	5.5509	5.6542
5	4.4723	4.5831	4.6928	4.8013	4.9089	5.0156	5.1214	5.2267	5.3311	5.4351	5.5385	5.6413
10	4.4483	4.5577	4.6661	4.7732	4.8796	4.9850	5.0894	5.1934	5.2965	5.3992	5.5013	5.6028
15	4.4088	4.5160	4.6222	4.7271	4.8312	4.9345	5.0367	5.1386	5.2395	5.3401	5.4401	5.5395
20	4.3545	4.4586	4.5617	4.6636	4.7648	4.8650	4.9644	5.0632	5.1613	5.2589	5.3560	5.4525
30	4.2050	4.3008	4.3957	4.4894	4.5824	4.6746	4.7660	4.8569	4.9470	5.0367	5.1259	5.2147
40	4.0095	4.0946	4.1790	4.2623	4.3449	4.4268	4.5079	4.5886	4.6687	4.7484	4.8276	4.9063
50	3.7799	3.8529	3.9251	3.9965	4.0673	4.1375	4.2071	4.2763	4.3448	4.4132	4.4810	4.5485
60	3.5292	3.5893	3.6489	3.7078	3.7662	3.8241	3.8815	3.9387	3.9953	4.0518	4.1079	4.1637
70	3.2701	3.3175	3.3646	3.4112	3.4574	3.5033	3.5488	3.5942	3.6392	3.6841	3.7287	3.7731
80	3.0141	3.0496	3.0850	3.1201	3.1550	3.1897	3.2243	3.2587	3.2930	3.3272	3.3613	3.3953
90	2.7707	2.7955	2.8204	2.8453	2.8702	2.8951	2.9199	2.9448	2.9697	2.9946	3.0194	3.0443
100	2.5470	2.5627	2.5786	2.5948	2.6112	2.6277	2.6444	2.6612	2.6781	2.6952	2.7123	2.7297
110	2.3476	2.3558	2.3644	2.3735	2.3829	2.3926	2.4026	2.4129	2.4235	2.4343	2.4452	2.4564
120	2.1754	2.1775	2.1803	2.1837	2.1876	2.1920	2.1968	2.2020	2.2076	2.2135	2.2197	2.2262
130	2.0312	2.0287	2.0270	2.0261	2.0258	2.0261	2.0270	2.0284	2.0302	2.0325	2.0350	2.0381
140	1.9150	1.9090	1.9040	1.8999	1.8966	1.8939	1.8919	1.8905	1.8896	1.8892	1.8891	1.8897
150	1.8261	1.8176	1.8103	1.8039	1.7984	1.7936	1.7896	1.7862	1.7835	1.7812	1.7794	1.7781
160	1.7635	1.7534	1.7445	1.7366	1.7297	1.7235	1.7182	1.7135	1.7095	1.7061	1.7031	1.7007
170	1.7263	1.7153	1.7055	1.6968	1.6890	1.6821	1.6761	1.6707	1.6660	1.6618	1.6582	1.6552
180	1.7140	1.7027	1.6926	1.6836	1.6756	1.6684	1.6621	1.6565	1.6516	1.6472	1.6434	1.6401
	2.5000	2.6000	2.7000	2.8000	2.9000	3.0000	3.1000	3.2000	3.3000	3.4000	3.5000	3.6000
0	5.7570	5.8594	5.9614	6.0631	6.1645	6.2654	6.3661	6.4664	6.5664	6.6664	6.7660	6.8654
5	5.7437	5.8456	5.9472	6.0485	6.1494	6.2499	6.3502	6.4500	6.5496	6.6492	6.7484	6.8473
10	5.7039	5.8045	5.9049	6.0049	6.1045	6.2038	6.3027	6.4014	6.4997	6.5980	6.6959	6.7936
15	5.6385	5.7370	5.8353	5.9332	6.0307	6.1279	6.2248	6.3213	6.4176	6.5138	6.6097	6.7053
20	5.5487	5.6443	5.7397	5.8347	5.9294	6.0237	6.1178	6.2115	6.3049	6.3983	6.4914	6.5842
30	5.3030	5.3908	5.4785	5.5657	5.6527	5.7393	5.8257	5.9118	5.9976	6.0833	6.1687	6.2539
40	4.9847	5.0627	5.1405	5.2179	5.2951	5.3719	5.4486	5.5249	5.6010	5.6770	5.7528	5.8283
50	4.6157	4.6825	4.7492	4.8155	4.8817	4.9475	5.0132	5.0786	5.1438	5.2089	5.2738	5.3385
60	4.2192	4.2745	4.3296	4.3844	4.4391	4.4936	4.5479	4.6020	4.6560	4.7099	4.7636	4.8172
70	3.8173	3.8614	3.9053	3.9491	3.9927	4.0362	4.0796	4.1228	4.1660	4.2091	4.2520	4.2949
80	3.4291	3.4629	3.4966	3.5303	3.5638	3.5974	3.6308	3.6641	3.6975	3.7308	3.7639	3.7971
90	3.0691	3.0940	3.1188	3.1437	3.1685	3.1934	3.2182	3.2431	3.2680	3.2929	3.3177	3.3425
100	2.7470	2.7644	2.7819	2.7995	2.8172	2.8349	2.8527	2.8706	2.8885	2.9064	2.9244	2.9425
110	2.4678	2.4793	2.4910	2.5028	2.5147	2.5269	2.5390	2.5514	2.5638	2.5764	2.5889	2.6017
120	2.2329	2.2399	2.2471	2.2545	2.2621	2.2699	2.2778	2.2860	2.2943	2.3027	2.3111	2.3199
130	2.0413	2.0450	2.0488	2.0529	2.0573	2.0619	2.0667	2.0718	2.0770	2.0824	2.0879	2.0936
140	1.8904	1.8916	1.8931	1.8948	1.8969	1.8993	1.9018	1.9047	1.9077	1.9110	1.9144	1.9180
150	1.7772	1.7767	1.7765	1.7766	1.7771	1.7779	1.7789	1.7803	1.7819	1.7836	1.7856	1.7878
160	1.6986	1.6971	1.6958	1.6949	1.6943	1.6942	1.6942	1.6946	1.6952	1.6960	1.6970	1.6983
170	1.6525	1.6503	1.6485	1.6470	1.6458	1.6451	1.6446	1.6444	1.6445	1.6448	1.6453	1.6461
180	1.6373	1.6349	1.6329	1.6312	1.6299	1.6290	1.6283	1.6279	1.6279	1.6280	1.6283	1.6289

TABLE IV (continued)

θ	Deuteron Energy											
	3.7000	3.8000	3.9000	4.0000	4.1000	4.2000	4.3000	4.4000	4.5000	4.6000	4.7000	4.8000
0	6.9646	7.0637	7.1624	7.2609	7.3595	7.4579	7.5560	7.6539	7.7519	7.8497	7.9472	8.0447
5	6.9462	7.0448	7.1431	7.2412	7.3394	7.4373	7.5350	7.6325	7.7300	7.8274	7.9245	8.0216
10	6.8912	6.9886	7.0856	7.1825	7.2794	7.3761	7.4725	7.5687	7.6650	7.7612	7.8570	7.9529
15	6.8008	6.8961	6.9911	7.0859	7.1808	7.2754	7.3698	7.4639	7.5582	7.6523	7.7461	7.8399
20	6.6769	6.7694	6.8616	6.9535	7.0456	7.1374	7.2290	7.3204	7.4119	7.5031	7.5942	7.6852
30	6.3390	6.4239	6.5085	6.5929	6.6774	6.7616	6.8457	6.9295	7.0134	7.0972	7.1807	7.2641
40	5.9038	5.9791	6.0541	6.1289	6.2038	6.2785	6.3530	6.4273	6.5017	6.5759	6.6499	6.7239
50	5.4032	5.4677	5.5319	5.5960	5.6602	5.7241	5.7879	5.8516	5.9153	5.9788	6.0422	6.1055
60	4.8707	4.9241	4.9772	5.0303	5.0834	5.1364	5.1892	5.2419	5.2946	5.3472	5.3997	5.4521
70	4.3376	4.3804	4.4229	4.4655	4.5080	4.5504	4.5927	4.6350	4.6772	4.7194	4.6715	4.8035
80	3.8302	3.8633	3.8963	3.9293	3.9623	3.9952	4.0281	4.0609	4.0938	4.1266	4.1594	4.1920
90	3.3674	3.3922	3.4170	3.4419	3.4668	3.4916	3.5164	3.5413	3.5661	3.5909	3.6158	3.6405
100	2.9605	2.9787	2.9968	3.0150	3.0333	3.0515	3.0699	3.0882	3.1065	3.1249	3.1433	3.1617
110	2.6144	2.6273	2.6402	2.6532	2.6664	2.6795	2.6927	2.7060	2.7193	2.7327	2.7461	2.7596
120	2.3286	2.3375	2.3465	2.3556	2.3649	2.3742	2.3836	2.3931	2.4026	2.4122	2.4220	2.4317
130	2.0995	2.1055	2.1116	2.1179	2.1243	2.1308	2.1374	2.1441	2.1509	2.1578	2.1649	2.1719
140	1.9218	1.9257	1.9298	1.9341	1.9385	1.9430	1.9477	1.9525	1.9573	1.9623	1.9675	1.9726
150	1.7901	1.7927	1.7954	1.7983	1.8014	1.8045	1.8079	1.8113	1.8149	1.8185	1.8224	1.8263
160	1.6997	1.7014	1.7032	1.7053	1.7075	1.7098	1.7123	1.7149	1.7176	1.7204	1.7235	1.7265
170	1.6470	1.6482	1.6495	1.6511	1.6528	1.6546	1.6566	1.6588	1.6610	1.6634	1.6660	1.6686
180	1.6297	1.6307	1.6319	1.6333	1.6348	1.6365	1.6384	1.6404	1.6425	1.6447	1.6471	1.6496

θ	4.9000	5.0000	5.1000	5.2000	5.3000	5.4000	5.5000	5.6000	5.7000	5.8000	5.9000	6.0000
0	8.1420	8.2394	8.3365	8.4336	8.5305	8.6273	8.7242	8.8208	8.9175	9.0140	9.1106	9.2069
5	8.1185	8.2155	8.3122	8.4088	8.5053	8.6017	8.6982	8.7944	8.8907	8.9867	9.0829	9.1788
10	8.0485	8.1443	8.2397	8.3351	8.4303	8.5255	8.6207	8.7157	8.8107	8.9055	9.0004	9.0951
15	7.9335	8.0272	8.1206	8.2140	8.3072	8.4003	8.4935	8.5864	8.6794	8.7722	8.8651	8.9577
20	7.7760	7.8669	7.9575	8.0481	8.1385	8.2289	8.3193	8.4095	8.4996	8.5897	8.6797	8.7696
30	7.3475	7.4309	7.5140	7.5970	7.6800	7.7628	7.8457	7.9284	8.0111	8.0936	8.1762	8.2586
40	6.7977	6.8716	6.9452	7.0188	7.0923	7.1657	7.2391	7.3124	7.3856	7.4587	7.5319	7.6049
50	6.1688	6.2320	6.2951	6.3581	6.4210	6.4838	6.5467	6.6094	6.6721	6.7347	6.7973	6.8598
60	5.5045	5.5569	5.6091	5.6613	5.7134	5.7654	5.8175	5.8694	5.9214	5.9732	6.0251	6.0768
70	4.8455	4.8875	4.9295	4.9713	5.0131	5.0549	5.0967	5.1384	5.1800	5.2217	5.2633	5.3048
80	4.2248	4.2575	4.2902	4.3228	4.3554	4.3880	4.4206	4.4531	4.4857	4.5182	4.5507	4.5832
90	3.6654	3.6903	3.7151	3.7399	3.7647	3.7895	3.8144	3.8392	3.8640	3.8888	3.9137	3.9385
100	3.1802	3.1987	3.2172	3.2357	3.2543	3.2729	3.2915	3.3101	3.3287	3.3473	3.3660	3.3847
110	2.7731	2.7867	2.8004	2.8140	2.8277	2.8414	2.8552	2.8690	2.8829	2.8968	2.9107	2.9246
120	2.4415	2.4515	2.4615	2.4714	2.4816	2.4917	2.5019	2.5122	2.5224	2.5328	2.5432	2.5536
130	2.1791	2.1864	2.1937	2.2011	2.2086	2.2162	2.2238	2.2315	2.2392	2.2470	2.2548	2.2628
140	1.9779	1.9833	1.9888	1.9944	2.0000	2.0058	2.0116	2.0175	2.0234	2.0294	2.0355	2.0416
150	1.8303	1.8345	1.8387	1.8430	1.8474	1.8519	1.8565	1.8612	1.8659	1.8707	1.8756	1.8805
160	1.7298	1.7331	1.7365	1.7400	1.7437	1.7474	1.7512	1.7551	1.7590	1.7630	1.7671	1.7713
170	1.6714	1.6743	1.6773	1.6803	1.6835	1.6868	1.6901	1.6936	1.6971	1.7007	1.7044	1.7082
180	1.6522	1.6550	1.6579	1.6607	1.6638	1.6670	1.6702	1.6735	1.6769	1.6803	1.6839	1.6875

θ	6.1000	6.2000	6.3000	6.4000	6.5000	6.6000	6.8000	7.0000	7.2000	7.4000	7.6000	7.8000
0	9.3031	9.3994	9.4956	9.5918	9.6878	9.7837	9.9756	10.1672	10.3586	10.5499	10.7409	10.9318
5	9.2745	9.3705	9.4662	9.5620	9.6576	9.7531	9.9441	10.1349	10.3255	10.5159	10.7061	10.8962
10	9.1896	9.2843	9.3788	9.4733	9.5677	9.6620	9.8505	10.0388	10.2270	10.4149	10.6026	10.7902
15	9.0502	9.1428	9.2353	9.3278	9.4201	9.5124	9.6969	9.8811	10.0652	10.2491	10.4327	10.6162
20	8.8593	8.9492	9.0389	9.1286	9.2182	9.3077	9.4866	9.6653	9.8439	10.0222	10.2003	10.3783
30	8.3409	8.4233	8.5055	8.5878	8.6698	8.7519	8.9159	9.0797	9.2433	9.4068	9.5700	9.7331
40	7.6777	7.7507	7.8235	7.8963	7.9690	8.0417	8.1869	8.3319	8.4768	8.6214	8.7659	8.9103
50	6.9221	6.9846	7.0469	7.1092	7.1715	7.2336	7.3579	7.4820	7.6060	7.7297	7.8534	7.9769
60	6.1284	6.1801	6.2318	6.2834	6.3349	6.3864	6.4894	6.5921	6.6948	6.7973	6.8997	7.0020
70	5.3463	5.3878	5.4293	5.4708	5.5122	5.5536	5.6363	5.7188	5.8013	5.8837	5.9661	6.0483
80	4.6156	4.6480	4.6805	4.7129	4.7453	4.7777	4.8424	4.9070	4.9716	5.0362	5.1007	5.1652
90	3.9632	3.9881	4.0129	4.0377	4.0625	4.0873	4.1370	4.1865	4.2361	4.2857	4.3353	4.3849
100	3.4033	3.4220	3.4408	3.4595	3.4782	3.4970	3.5345	3.5720	3.6097	3.6473	3.6851	3.7228
110	2.9386	2.9526	2.9666	2.9806	2.9947	3.0089	3.0372	3.0655	3.0939	3.1224	3.1511	3.1798
120	2.5641	2.5746	2.5852	2.5957	2.6064	2.6171	2.6385	2.6600	2.6817	2.7035	2.7254	2.7474
130	2.2707	2.2787	2.2868	2.2949	2.3030	2.3112	2.3278	2.3444	2.3612	2.3781	2.3953	2.4125
140	2.0478	2.0540	2.0604	2.0667	2.0731	2.0796	2.0927	2.1059	2.1193	2.1329	2.1467	2.1605
150	1.8855	1.8905	1.8957	1.9008	1.9061	1.9114	1.9222	1.9331	1.9442	1.9555	1.9670	1.9786
160	1.7755	1.7798	1.7842	1.7886	1.7931	1.7977	1.8070	1.8164	1.8260	1.8359	1.8459	1.8561
170	1.7120	1.7158	1.7198	1.7238	1.7279	1.7320	1.7405	1.7491	1.7579	1.7669	1.7762	1.7855
180	1.6912	1.6949	1.6988	1.7026	1.7066	1.7106	1.7188	1.7271	1.7357	1.7444	1.7534	1.7625

TABLE IV (continued)

θ	Deuteron Energy 8.0000	8.5000	9.0000	9.5000	10.0000	10.5000	11.0000	11.5000	12.0000	12.5000	13.0000	13.5000
0	11.1226	11.5987	12.0742	12.5489	13.0230	13.4967	13.9698	14.4425	14.9147	15.3867	15.8585	16.3298
5	11.0861	11.5602	12.0336	12.5062	12.9783	13.4498	13.9209	14.3915	14.8616	15.3316	15.8012	16.2705
10	10.9777	11.4456	11.9128	12.3792	12.8450	13.3104	13.7753	14.2398	14.7037	15.1674	15.6309	16.0940
15	10.7997	11.2574	11.7145	12.1708	12.6265	13.0818	13.5365	13.9909	14.4446	14.8982	15.3516	15.8045
20	10.5562	11.0002	11.4434	11.8859	12.3278	12.7693	13.2102	13.6507	14.0907	14.5305	14.9700	15.4091
30	9.8961	10.3029	10.7089	11.1143	11.5190	11.9233	12.3271	12.7305	13.1333	13.5360	13.9383	14.3403
40	9.0546	9.4145	9.7739	10.1325	10.4906	10.8481	11.2053	11.5620	11.9183	12.2743	12.6300	12.9854
50	8.1003	8.4082	8.7156	9.0223	9.3285	9.6343	9.9396	10.2446	10.5492	10.8535	11.1575	11.4612
60	7.1042	7.3593	7.6138	7.8678	8.1214	8.3746	8.6274	8.8800	9.1321	9.3841	9.6358	9.8873
70	6.1305	6.3356	6.5403	6.7447	6.9487	7.1524	7.3558	7.5591	7.7620	7.9648	8.1674	8.3698
80	5.2296	5.3905	5.5512	5.7116	5.8719	6.0320	6.1919	6.3518	6.5114	6.6709	6.8304	6.9897
90	4.4345	4.5584	4.6823	4.8062	4.9301	5.0538	5.1776	5.3013	5.4250	5.5487	5.6723	5.7959
100	3.7605	3.8551	3.9498	4.0446	4.1396	4.2346	4.3298	4.4250	4.5203	4.6157	4.7111	4.8065
110	3.2085	3.2807	3.3531	3.4259	3.4989	3.5721	3.6456	3.7193	3.7931	3.8670	3.9410	4.0152
120	2.7695	2.8252	2.8813	2.9378	2.9948	3.0519	3.1095	3.1673	3.2253	3.2836	3.3420	3.4006
130	2.4298	2.4736	2.5180	2.5630	2.6084	2.6541	2.7003	2.7468	2.7936	2.8406	2.8878	2.9353
140	2.1745	2.2101	2.2463	2.2831	2.3205	2.3583	2.3965	2.4351	2.4740	2.5132	2.5527	2.5924
150	1.9903	2.0203	2.0510	2.0823	2.1142	2.1466	2.1794	2.2127	2.2463	2.2802	2.3144	2.3488
160	1.8664	1.8928	1.9200	1.9478	1.9762	2.0051	2.0345	2.0644	2.0946	2.1251	2.1559	2.1870
170	1.7951	1.8195	1.8447	1.8706	1.8971	1.9241	1.9516	1.9795	2.0078	2.0364	2.0653	2.0946
180	1.7718	1.7956	1.8202	1.8454	1.8713	1.8977	1.9246	1.9519	1.9796	2.0076	2.0359	2.0645

θ	14.0000	14.5000	15.0000	16.0000	17.0000	18.0000	19.0000	20.0000	21.0000	22.0000	23.0000	24.0000
0	16.8009	17.2718	17.7426	18.6834	19.6237	20.5633	21.5025	22.4413	23.3799	24.3181	25.2559	26.1937
5	16.7395	17.2083	17.6771	18.6136	19.5498	20.4852	21.4202	22.3548	23.2892	24.2232	25.1569	26.0904
10	16.5568	17.0194	17.4819	18.4061	19.3298	20.2528	21.1754	22.0976	23.0195	23.9410	24.8622	25.7833
15	16.2572	16.7097	17.1620	18.0659	18.9693	19.8719	20.7742	21.6760	22.5775	23.4787	24.3795	25.2801
20	15.8480	16.2866	16.7252	17.6014	18.4771	19.3520	20.2266	21.1007	21.9744	22.8478	23.7208	24.5936
30	14.7420	15.1435	15.5449	16.3467	17.1480	17.9486	18.7486	19.5483	20.3474	21.1462	21.9446	22.7427
40	13.3405	13.6954	14.0501	14.7588	15.4668	16.1741	16.8809	17.5872	18.2930	18.9985	19.7034	20.4081
50	11.7647	12.0679	12.3710	12.9765	13.5813	14.1855	14.7891	15.3922	15.9948	16.5971	17.1988	17.8003
60	10.1385	10.3896	10.6404	11.1416	11.6422	12.1421	12.6417	13.1407	13.6393	14.1374	14.6352	15.1327
70	8.5721	8.7742	8.9761	9.3795	9.7825	10.1850	10.5871	10.9888	11.3902	11.7912	12.1918	12.5922
80	7.1489	7.3080	7.4670	7.7848	8.1022	8.4194	8.7362	9.0528	9.3691	9.6852	10.0011	10.3167
90	5.9195	6.0430	6.1665	6.4134	6.6601	6.9068	7.1533	7.3997	7.6459	7.8921	8.1381	8.3839
100	4.9021	4.9976	5.0931	5.2843	5.4755	5.6668	5.8582	6.0495	6.2408	6.4321	6.6233	6.8146
110	4.0895	4.1639	4.2383	4.3874	4.5368	4.6864	4.8361	4.9860	5.1359	5.2859	5.4361	5.5862
120	3.4594	3.5183	3.5773	3.6956	3.8144	3.9335	4.0529	4.1724	4.2922	4.4121	4.5322	4.6523
130	2.9830	3.0309	3.0788	3.1753	3.2722	3.3695	3.4672	3.5652	3.6634	3.7618	3.8605	3.9592
140	2.6324	2.6725	2.7128	2.7939	2.8755	2.9577	3.0403	3.1231	3.2063	3.2897	3.3733	3.4571
150	2.3836	2.4185	2.4535	2.5242	2.5955	2.6674	2.7396	2.8123	2.8852	2.9584	3.0318	3.1055
160	2.2183	2.2499	2.2816	2.3456	2.4103	2.4755	2.5412	2.6072	2.6735	2.7402	2.8071	2.8742
170	2.1240	2.1537	2.1836	2.2439	2.3049	2.3664	2.4284	2.4907	2.5534	2.6164	2.6797	2.7431
180	2.0934	2.1225	2.1518	2.2109	2.2707	2.3310	2.3918	2.4530	2.5145	2.5763	2.6384	2.7007

θ	25.0000
0	27.1312
5	27.0238
10	26.7041
15	26.1805
20	25.4661
30	23.5405
40	21.1124
50	18.4013
60	15.6298
70	12.9923
80	10.6321
90	8.6296
100	7.0057
110	5.7364
120	4.7726
130	4.0581
140	3.5411
150	3.1793
160	2.9415
170	2.8068
180	2.7631

TABLE V

$D + H^3 \longrightarrow He^4 + n$

$2.0147400 + 3.0170050 \longrightarrow 4.0038730 + 1.0089861$

θ	Deuteron Energy											
	0.1000	0.2000	0.3000	0.4000	0.5000	0.6000	0.7000	0.8000	0.9000	1.0000	1.1000	1.2000
0	14.7569	15.0937	15.3671	15.6064	15.8254	16.0289	16.2212	16.4053	16.5815	16.7523	16.9175	17.0784
5	14.7542	15.0898	15.3623	15.6007	15.8190	16.0218	16.2134	16.3969	16.5725	16.7428	16.9074	17.0678
10	14.7462	15.0782	15.3478	15.5838	15.7998	16.0005	16.1903	16.3718	16.5457	16.7143	16.8773	17.0361
15	14.7329	15.0589	15.3238	15.5557	15.7681	15.9653	16.1519	16.3304	16.5014	16.6672	16.8275	16.9836
20	14.7143	15.0322	15.2906	15.5168	15.7240	15.9166	16.0987	16.2730	16.4400	16.6019	16.7585	16.9110
30	14.6625	14.9574	15.1975	15.4081	15.6010	15.7805	15.9503	16.1129	16.2687	16.4199	16.5662	16.7087
40	14.5923	14.8565	15.0722	15.2617	15.4356	15.5975	15.7510	15.8980	16.0391	16.1760	16.3086	16.4379
50	14.5064	14.7331	14.9191	15.0831	15.2340	15.3749	15.5087	15.6371	15.7604	15.8802	15.9965	16.1099
60	14.4074	14.5914	14.7436	14.8788	15.0038	15.1209	15.2326	15.3400	15.4435	15.5443	15.6422	15.7380
70	14.2987	14.4362	14.5519	14.6560	14.7530	14.8448	14.9328	15.0178	15.1002	15.1807	15.2593	15.3364
80	14.1837	14.2725	14.3503	14.4221	14.4904	14.5561	14.6197	14.6819	14.7428	14.8026	14.8615	14.9197
90	14.0661	14.1058	14.1454	14.1849	14.2245	14.2641	14.3038	14.3434	14.3829	14.4225	14.4621	14.5017
100	13.9495	13.9409	13.9434	13.9517	13.9635	13.9781	13.9947	14.0127	14.0320	14.0523	14.0735	14.0955
110	13.8374	13.7830	13.7503	13.7292	13.7151	13.7063	13.7015	13.6994	13.7000	13.7024	13.7068	13.7127
120	13.7330	13.6364	13.5716	13.5237	13.4860	13.4562	13.4320	13.4119	13.3957	13.3823	13.3716	13.3632
130	13.6394	13.5053	13.4121	13.3407	13.2824	13.2342	13.1932	13.1574	13.1267	13.0995	13.0759	13.0552
140	13.5591	13.3932	13.2760	13.1847	13.1091	13.0455	12.9905	12.9418	12.8990	12.8604	12.8261	12.7951
150	13.4942	13.3029	13.1666	13.0596	12.9703	12.8945	12.8284	12.7695	12.7172	12.6697	12.6270	12.5882
160	13.4467	13.2368	13.0866	12.9682	12.8690	12.7844	12.7103	12.6441	12.5850	12.5311	12.4825	12.4379
170	13.4177	13.1965	13.0378	12.9125	12.8073	12.7175	12.6386	12.5679	12.5047	12.4470	12.3948	12.3468
180	13.4079	13.1829	13.0214	12.8938	12.7866	12.6950	12.6145	12.5423	12.4778	12.4189	12.3654	12.3163
	1.3000	1.4000	1.5000	1.6000	1.7000	1.8000	1.9000	2.0000	2.1000	2.2000	2.3000	2.4000
0	17.2359	17.3896	17.5403	17.6887	17.8346	17.9780	18.1194	18.2589	18.3970	18.5332	18.6680	18.8018
5	17.2248	17.3779	17.5281	17.6761	17.8215	17.9644	18.1053	18.2444	18.3821	18.5179	18.6522	18.7855
10	17.1915	17.3432	17.4919	17.6384	17.7824	17.9239	18.0635	18.2012	18.3375	18.4720	18.6051	18.7371
15	17.1365	17.2857	17.4320	17.5761	17.7178	17.8570	17.9943	18.1297	18.2639	18.3962	18.5271	18.6570
20	17.0603	17.2061	17.3491	17.4898	17.6283	17.7644	17.8985	18.0309	18.1621	18.2914	18.4193	18.5463
30	16.8482	16.9845	17.1182	17.2499	17.3794	17.5067	17.6323	17.7562	17.8790	18.0001	18.1199	18.2388
40	16.5645	16.6882	16.8097	16.9293	17.0471	17.1628	17.2771	17.3899	17.5016	17.6119	17.7210	17.8293
50	16.2211	16.3299	16.4368	16.5421	16.6458	16.7479	16.8487	16.9483	17.0469	17.1444	17.2409	17.3367
60	15.8321	15.9242	16.0149	16.1044	16.1926	16.2795	16.3654	16.4504	16.5347	16.6180	16.7006	16.7826
70	15.4124	15.4870	15.5606	15.6333	15.7052	15.7763	15.8466	15.9163	15.9855	16.0541	16.1221	16.1898
80	14.9772	15.0341	15.0905	15.1464	15.2018	15.2569	15.3116	15.3660	15.4201	15.4739	15.5275	15.5808
90	14.5413	14.5809	14.6205	14.6600	14.6996	14.7392	14.7788	14.8184	14.8579	14.8975	14.9371	14.9766
100	14.1181	14.1414	14.1653	14.1895	14.2140	14.2392	14.2646	14.2904	14.3164	14.3427	14.3693	14.3961
110	13.7198	13.7282	13.7376	13.7478	13.7588	13.7708	13.7834	13.7967	13.8104	13.8248	13.8398	13.8551
120	13.3565	13.3517	13.3483	13.3462	13.3452	13.3456	13.3470	13.3494	13.3524	13.3564	13.3611	13.3664
130	13.0366	13.0205	13.0063	12.9936	12.9825	12.9730	12.9649	12.9580	12.9519	12.9471	12.9432	12.9400
140	12.7668	12.7414	12.7183	12.6970	12.6775	12.6601	12.6442	12.6297	12.6162	12.6042	12.5934	12.5834
150	12.5523	12.5197	12.4896	12.4616	12.4357	12.4120	12.3901	12.3698	12.3506	12.3332	12.3170	12.3017
160	12.3966	12.3588	12.3238	12.2911	12.2606	12.2325	12.2063	12.1819	12.1587	12.1373	12.1174	12.0984
170	12.3023	12.2614	12.2235	12.1879	12.1546	12.1239	12.0952	12.0683	12.0427	12.0191	11.9968	11.9757
180	12.2707	12.2288	12.1898	12.1533	12.1191	12.0876	12.0580	12.0303	12.0039	11.9795	11.9565	11.9346
	2.5000	2.6000	2.7000	2.8000	2.9000	3.0000	3.1000	3.2000	3.3000	3.4000	3.5000	3.6000
0	18.9339	19.0652	19.1950	19.3237	19.4519	19.5788	19.7047	19.8301	19.9545	20.0783	20.2013	20.3234
5	18.9172	19.0481	19.1775	19.3058	19.4336	19.5601	19.6856	19.8106	19.9345	20.0580	20.1806	20.3023
10	18.8675	18.9971	19.1253	19.2524	19.3789	19.5042	19.6285	19.7523	19.8751	19.9974	20.1187	20.2394
15	18.7854	18.9129	19.0390	19.1641	19.2886	19.4118	19.5342	19.6561	19.7768	19.8972	20.0166	20.1354
20	18.6718	18.7964	18.9198	19.0420	19.1638	19.2843	19.4039	19.5230	19.6411	19.7588	19.8756	19.9917
30	18.3563	18.4731	18.5887	18.7032	18.8173	18.9302	19.0424	19.1540	19.2648	19.3751	19.4846	19.5934
40	17.9364	18.0428	18.1482	18.2526	18.3567	18.4597	18.5620	18.6639	18.7649	18.8656	18.9656	19.0650
50	17.4315	17.5257	17.6190	17.7115	17.8037	17.8951	17.9858	18.0762	18.1659	18.2553	18.3440	18.4323
60	16.8638	16.9446	17.0247	17.1042	17.1834	17.2620	17.3400	17.4178	17.4951	17.5721	17.6486	17.7247
70	16.2569	16.3237	16.3901	16.4559	16.5217	16.5870	16.6520	16.7167	16.7810	16.8453	16.9092	16.9728
80	15.6338	15.6867	15.7394	15.7918	15.8442	15.8963	15.9483	16.0001	16.0517	16.1033	16.1547	16.2060
90	15.0162	15.0557	15.0953	15.1348	15.1745	15.2140	15.2536	15.2931	15.3326	15.3722	15.4118	15.4513
100	14.4231	14.4504	14.4778	14.5054	14.5333	14.5613	14.5894	14.6176	14.6460	14.6745	14.7033	14.7321
110	13.8709	13.8870	13.9036	13.9206	13.9379	13.9556	13.9735	13.9917	14.0102	14.0289	14.0480	14.0673
120	13.3724	13.3789	13.3862	13.3939	13.4021	13.4108	13.4200	13.4294	13.4394	13.4497	13.4605	13.4716
130	12.9378	12.9363	12.9356	12.9356	12.9361	12.9374	12.9392	12.9414	12.9443	12.9475	12.9515	12.9557
140	12.5746	12.5665	12.5594	12.5532	12.5476	12.5428	12.5388	12.5351	12.5323	12.5299	12.5283	12.5271
150	12.2878	12.2746	12.2627	12.2517	12.2414	12.2321	12.2235	12.2154	12.2083	12.2016	12.1958	12.1905
160	12.0809	12.0642	12.0489	12.0345	12.0209	12.0083	11.9966	11.9854	11.9752	11.9656	11.9568	11.9486
170	11.9560	11.9372	11.9199	11.9035	11.8879	11.8735	11.8599	11.8468	11.8348	11.8234	11.8129	11.8030
180	11.9142	11.8948	11.8768	11.8597	11.8435	11.8284	11.8142	11.8006	11.7880	11.7759	11.7649	11.7544

TABLE V (continued)

θ	Deuteron Energy											
	3.7000	3.8000	3.9000	4.0000	4.1000	4.2000	4.3000	4.4000	4.5000	4.6000	4.7000	4.8000
0	20.4452	20.5662	20.6864	20.8065	20.9256	21.0443	21.1628	21.2804	21.3976	21.5144	21.6310	21.7469
5	20.4237	20.5443	20.6642	20.7839	20.9026	21.0209	21.1390	21.2563	21.3731	21.4896	21.6057	21.7213
10	20.3596	20.4790	20.5978	20.7163	20.8339	20.9511	21.0681	21.1843	21.3000	21.4153	21.5304	21.6449
15	20.2537	20.3712	20.4881	20.6047	20.7205	20.8358	20.9510	21.0653	21.1792	21.2927	21.4059	21.5186
20	20.1074	20.2223	20.3366	20.4507	20.5639	20.6767	20.7893	20.9011	21.0124	21.1235	21.2342	21.3444
30	19.7019	19.8097	19.9169	20.0239	20.1300	20.2358	20.3414	20.4463	20.5508	20.6550	20.7589	20.8623
40	19.1640	19.2625	19.3604	19.4581	19.5551	19.6518	19.7483	19.8441	19.9396	20.0349	20.1298	20.2244
50	18.5203	18.6078	18.6948	18.7817	18.8679	18.9539	19.0397	19.1250	19.2100	19.2948	19.3793	19.4635
60	17.8007	17.8762	17.9514	18.0264	18.1010	18.1753	18.2496	18.3234	18.3970	18.4704	18.5436	18.6165
70	17.0362	17.0995	17.1624	17.2253	17.2878	17.3502	17.4125	17.4745	17.5364	17.5981	17.6597	17.7211
80	16.2571	16.3082	16.3592	16.4100	16.4607	16.5114	16.5620	16.6124	16.6628	16.7131	16.7633	16.8135
90	15.4908	15.5304	15.5700	15.6095	15.6490	15.6886	15.7281	15.7676	15.8072	15.8468	15.8862	15.9258
100	14.7609	14.7900	14.8191	14.8483	14.8776	14.9071	14.9366	14.9662	14.9959	15.0257	15.0554	15.0854
110	14.0867	14.1064	14.1264	14.1464	14.1667	14.1873	14.2079	14.2288	14.2498	14.2710	14.2922	14.3137
120	13.4829	13.4947	13.5067	13.5190	13.5315	13.5445	13.5575	13.5709	13.5846	13.5985	13.6124	13.6268
130	12.9603	12.9655	12.9710	12.9768	12.9830	12.9896	12.9964	13.0037	13.0112	13.0191	13.0271	13.0355
140	12.5263	12.5262	12.5265	12.5271	12.5283	12.5299	12.5318	12.5341	12.5368	12.5399	12.5431	12.5469
150	12.1856	12.1815	12.1779	12.1746	12.1719	12.1697	12.1678	12.1664	12.1655	12.1650	12.1646	12.1649
160	11.9409	11.9340	11.9276	11.9215	11.9162	11.9114	11.9068	11.9029	11.8994	11.8965	11.8936	11.8914
170	11.7936	11.7850	11.7770	11.7694	11.7624	11.7561	11.7500	11.7446	11.7396	11.7351	11.7308	11.7272
180	11.7444	11.7353	11.7268	11.7186	11.7111	11.7042	11.6977	11.6918	11.6863	11.6813	11.6765	11.6724
	4.9000	5.0000	5.1000	5.2000	5.3000	5.4000	5.5000	5.6000	5.7000	5.8000	5.9000	6.0000
0	21.8626	21.9778	22.0925	22.2072	22.3212	22.4349	22.5483	22.6615	22.7742	22.8867	22.9991	23.1110
5	21.8367	21.9514	22.0658	22.1801	22.2938	22.4071	22.5201	22.6330	22.7454	22.8575	22.9696	23.0811
10	21.7591	21.8728	21.9861	22.0993	22.2119	22.3242	22.4361	22.5480	22.6592	22.7703	22.8813	22.9918
15	21.6311	21.7430	21.8545	21.9659	22.0768	22.1872	22.2974	22.4075	22.5170	22.6264	22.7357	22.8444
20	21.4544	21.5638	21.6729	21.7819	21.8903	21.9983	22.1061	22.2138	22.3209	22.4279	22.5347	22.6411
30	20.9655	21.0681	21.1705	21.2727	21.3745	21.4759	21.5770	21.6781	21.7786	21.8790	21.9793	22.0791
40	20.3187	20.4126	20.5062	20.5997	20.6928	20.7855	20.8781	20.9705	21.0625	21.1543	21.2461	21.3374
50	19.5475	19.6312	19.7146	19.7978	19.8808	19.9634	20.0459	20.1283	20.2103	20.2922	20.3740	20.4555
60	18.6893	18.7618	18.8342	18.9064	18.9783	19.0501	19.1217	19.1932	19.2644	19.3356	19.4067	19.4775
70	17.7824	17.8435	17.9045	17.9654	18.0262	18.0868	18.1473	18.2077	18.2679	18.3281	18.3882	18.4482
80	16.8635	16.9135	16.9634	17.0132	17.0631	17.1128	17.1624	17.2120	17.2615	17.3111	17.3605	17.4099
90	15.9652	16.0048	16.0444	16.0838	16.1234	16.1629	16.2024	16.2419	16.2814	16.3209	16.3605	16.3999
100	15.1153	15.1453	15.1755	15.2056	15.2359	15.2662	15.2966	15.3269	15.3573	15.3879	15.4185	15.4491
110	14.3352	14.3570	14.3789	14.4008	14.4230	14.4452	14.4676	14.4900	14.5125	14.5353	14.5580	14.5809
120	13.6411	13.6559	13.6708	13.6857	13.7010	13.7164	13.7321	13.7477	13.7636	13.7797	13.7959	13.8122
130	13.0440	13.0529	13.0621	13.0714	13.0810	13.0909	13.1010	13.1111	13.1215	13.1323	13.1430	13.1540
140	12.5507	12.5551	12.5597	12.5645	12.5697	12.5751	12.5809	12.5866	12.5928	12.5993	12.6058	12.6126
150	12.1652	12.1661	12.1674	12.1687	12.1706	12.1727	12.1752	12.1777	12.1806	12.1839	12.1872	12.1910
160	11.8893	11.8878	11.8867	11.8857	11.8852	11.8851	11.8853	11.8855	11.8862	11.8873	11.8885	11.8900
170	11.7237	11.7208	11.7183	11.7159	11.7141	11.7126	11.7114	11.7104	11.7097	11.7095	11.7094	11.7097
180	11.6684	11.6651	11.6621	11.6593	11.6570	11.6551	11.6535	11.6520	11.6510	11.6503	11.6498	11.6496
	6.1000	6.2000	6.3000	6.4000	6.5000	6.6000	6.8000	7.0000	7.2000	7.4000	7.6000	7.8000
0	23.2226	23.3342	23.4452	23.5561	23.6669	23.7772	23.9972	24.2166	24.4351	24.6529	24.8696	25.0859
5	23.1923	23.3036	23.4142	23.5248	23.6353	23.7452	23.9645	24.1832	24.4010	24.6181	24.8341	25.0498
10	23.1019	23.2122	23.3218	23.4312	23.5407	23.6496	23.8669	24.0835	24.2993	24.5143	24.7283	24.9419
15	22.9528	23.0613	23.1692	23.2770	23.3847	23.4919	23.7057	23.9190	24.1314	24.3431	24.5537	24.7639
20	22.7471	22.8532	22.9588	23.0642	23.1696	23.2744	23.4836	23.6922	23.8999	24.1070	24.3130	24.5186
30	22.1787	22.2783	22.3773	22.4763	22.5752	22.6737	22.8700	23.0659	23.2609	23.4553	23.6487	23.8418
40	21.4285	21.5197	21.6103	21.7009	21.7914	21.8816	22.0613	22.2406	22.4191	22.5971	22.7743	22.9511
50	20.5368	20.6181	20.6990	20.7798	20.8606	20.9410	21.1015	21.2615	21.4209	21.5799	21.7381	21.8961
60	19.5481	19.6188	19.6891	19.7595	19.8297	19.8997	20.0394	20.1787	20.3176	20.4561	20.5940	20.7316
70	18.5080	18.5679	18.6274	18.6871	18.7466	18.8060	18.9245	19.0428	19.1608	19.2785	19.3958	19.5129
80	17.4592	17.5086	17.5577	17.6070	17.6561	17.7052	17.8032	17.9012	17.9989	18.0965	18.1939	18.2912
90	16.4395	16.4790	16.5184	16.5580	16.5975	16.6370	16.7159	16.7950	16.8739	16.9529	17.0318	17.1108
100	15.4798	15.5105	15.5412	15.5720	15.6028	15.6337	15.6956	15.7577	15.8198	15.8822	15.9446	16.0072
110	14.6039	14.6269	14.6500	14.6734	14.6966	14.7201	14.7671	14.8145	14.8621	14.9101	14.9583	15.0067
120	13.8287	13.8453	13.8620	13.8790	13.8959	13.9131	13.9477	13.9828	14.0182	14.0541	14.0904	14.1270
130	13.1653	13.1766	13.1881	13.1999	13.2117	13.2237	13.2482	13.2733	13.2988	13.3249	13.3516	13.3786
140	12.6197	12.6269	12.6343	12.6420	12.6497	12.6578	12.6744	12.6916	12.7094	12.7279	12.7470	12.7666
150	12.1949	12.1990	12.2034	12.2081	12.2128	12.2178	12.2285	12.2399	12.2520	12.2648	12.2783	12.2923
160	11.8918	11.8938	11.8960	11.8986	11.9012	11.9042	11.9109	11.9182	11.9263	11.9352	11.9449	11.9551
170	11.7102	11.7109	11.7119	11.7133	11.7147	11.7165	11.7208	11.7258	11.7316	11.7382	11.7456	11.7536
180	11.6498	11.6501	11.6507	11.6516	11.6526	11.6540	11.6575	11.6617	11.6668	11.6726	11.6793	11.6866

TABLE V (continued)

θ	Deuteron Energy											
	8.0000	8.5000	9.0000	9.5000	10.0000	10.5000	11.0000	11.5000	12.0000	12.5000	13.0000	13.5000
0	25.3013	25.8371	26.3695	26.8985	27.4244	27.9478	28.4686	28.9871	29.5036	30.0181	30.5312	31.0424
5	25.2645	25.7986	26.3293	26.8566	27.3809	27.9026	28.4217	28.9387	29.4535	29.9664	30.4779	30.9875
10	25.1546	25.6837	26.2094	26.7317	27.2510	27.7679	28.2821	28.7941	29.3041	29.8122	30.3189	30.8236
15	24.9733	25.4941	26.0116	26.5257	27.0370	27.5457	28.0519	28.5559	29.0579	29.5580	30.0568	30.5536
20	24.7234	25.2329	25.7391	26.2420	26.7421	27.2398	27.7349	28.2280	28.7190	29.2082	29.6961	30.1821
30	24.0341	24.5125	24.9879	25.4602	25.9298	26.3972	26.8622	27.3253	27.7865	28.2460	28.7042	29.1607
40	23.1272	23.5654	24.0008	24.4336	24.8639	25.2922	25.7183	26.1428	26.5655	26.9867	27.4067	27.8252
50	22.0535	22.4451	22.8343	23.2213	23.6062	23.9894	24.3707	24.7506	25.1290	25.5061	25.8821	26.2569
60	20.8689	21.2106	21.5503	21.8883	22.2246	22.5595	22.8930	23.2254	23.5565	23.8866	24.2159	24.5441
70	19.6298	19.9209	20.2106	20.4992	20.7866	21.0729	21.3583	21.6429	21.9266	22.2096	22.4920	22.7737
80	18.3884	18.6308	18.8724	19.1135	19.3539	19.5937	19.8331	20.0720	20.3104	20.5485	20.7862	21.0236
90	17.1898	17.3871	17.5844	17.7817	17.9789	18.1760	18.3731	18.5703	18.7673	18.9643	19.1613	19.3582
100	16.0700	16.2272	16.3850	16.5435	16.7025	16.8619	17.0217	17.1819	17.3425	17.5034	17.6646	17.8260
110	15.0555	15.1782	15.3022	15.4274	15.5536	15.6807	15.8087	15.9376	16.0671	16.1973	16.3281	16.4594
120	14.1641	14.2581	14.3538	14.4514	14.5505	14.6509	14.7526	14.8555	14.9594	15.0643	15.1702	15.2768
130	13.4063	13.4770	13.5501	13.6254	13.7027	13.7816	13.8623	13.9445	14.0280	14.1128	14.1987	14.2857
140	12.7869	12.8396	12.8950	12.9531	13.0135	13.0758	13.1402	13.2064	13.2742	13.3434	13.4140	13.4859
150	12.3072	12.3464	12.3887	12.4341	12.4820	12.5321	12.5845	12.6390	12.6951	12.7530	12.8123	12.8731
160	11.9662	11.9962	12.0296	12.0662	12.1056	12.1474	12.1916	12.2380	12.2863	12.3363	12.3880	12.4413
170	11.7625	11.7872	11.8153	11.8469	11.8813	11.9182	11.9577	11.9994	12.0431	12.0887	12.1359	12.1848
180	11.6948	11.7177	11.7441	11.7740	11.8068	11.8421	11.8800	11.9202	11.9624	12.0065	12.0523	12.0998
	14.0000	14.5000	15.0000	16.0000	17.0000	18.0000	19.0000	20.0000	21.0000	22.0000	23.0000	24.0000
0	31.5521	32.0601	32.5672	33.5776	34.5837	35.5858	36.5847	37.5807	38.5739	39.5644	40.5530	41.5396
5	31.4955	32.0020	32.5074	33.5146	34.5176	35.5165	36.5122	37.5051	38.4951	39.4825	40.4679	41.4514
10	31.3269	31.8286	32.3292	33.3269	34.3204	35.3098	36.2961	37.2795	38.2602	39.2382	40.2142	41.1884
15	31.0490	31.5428	32.0357	33.0177	33.9956	34.9695	35.9403	36.9083	37.8734	38.8361	39.7967	40.7555
20	30.6667	31.1497	31.6318	32.5924	33.5489	34.5016	35.4511	36.3979	37.3420	38.2835	39.2231	40.1608
30	29.6159	30.0696	30.5224	31.4245	32.3229	33.2177	34.1095	34.9986	35.8852	36.7694	37.6516	38.5321
40	28.2424	28.6584	29.0735	29.9006	30.7243	31.5447	32.3623	33.1776	33.9904	34.8011	35.6100	36.4173
50	26.6306	27.0031	27.3750	28.1160	28.8540	29.5892	30.3219	31.0526	31.7812	32.5078	33.2329	33.9565
60	24.8715	25.1980	25.5239	26.1736	26.8208	27.4657	28.1087	28.7499	29.3894	30.0274	30.6640	31.2995
70	23.0547	23.3352	23.6152	24.1737	24.7304	25.2854	25.8391	26.3915	26.9427	27.4927	28.0417	28.5898
80	21.2606	21.4972	21.7337	22.2056	22.6767	23.1467	23.6160	24.0845	24.5524	25.0195	25.4860	25.9521
90	19.5551	19.7519	19.9488	20.3422	20.7355	21.1286	21.5216	21.9144	22.3070	22.6995	23.0918	23.4839
100	17.9877	18.1497	18.3119	18.6367	18.9622	19.2882	19.6149	19.9418	20.2692	20.5970	20.9249	21.2531
110	16.5913	16.7237	16.8566	17.1235	17.3919	17.6615	17.9323	18.2041	18.4767	18.7502	19.0243	19.2991
120	15.3843	15.4925	15.6014	15.8208	16.0425	16.2661	16.4916	16.7183	16.9466	17.1760	17.4065	17.6379
130	14.3737	14.4626	14.5525	14.7344	14.9191	15.1064	15.2959	15.4872	15.6804	15.8752	16.0713	16.2687
140	13.5590	13.6332	13.7084	13.8615	14.0180	14.1774	14.3396	14.5039	14.6703	14.8387	15.0087	15.1802
150	12.9352	12.9986	13.0632	13.1952	13.3310	13.4702	13.6123	13.7569	13.9039	14.0530	14.2039	14.3566
160	12.4959	12.5520	12.6093	12.7270	12.8488	12.9742	13.1028	13.2340	13.3678	13.5040	13.6420	13.7819
170	12.2351	12.2869	12.3400	12.4495	12.5632	12.6806	12.8014	12.9249	13.0511	13.1797	13.3103	13.4428
180	12.1487	12.1991	12.2508	12.3576	12.4686	12.5834	12.7016	12.8226	12.9463	13.0725	13.2007	13.3308
	25.0000											
0	42.5242											
5	42.4329											
10	42.1605											
15	41.7122											
20	41.0965											
30	39.4108											
40	37.2228											
50	34.6786											
60	31.9337											
70	29.1370											
80	26.4175											
90	23.8759											
100	21.5816											
110	19.5745											
120	17.8703											
130	16.4673											
140	15.3531											
150	14.5108											
160	13.9235											
170	13.5772											
180	13.4628											

Case C: $(\alpha_1=1)$

In the limiting case, $\theta_{max}=\pi/2$ and the positive sign is always used. The negative sign gives the redundant root $\cos\Omega=-1$.

The Jacobian which transforms the solid angle from the laboratory system to the c.m. system is obtained by taking the ratio of the differentials

$$J(\omega_n)=\frac{d(\cos\omega_n)}{d(\cos\Omega)} \quad \text{where} \quad \omega_1=\theta \quad \text{and} \quad \omega_2=\phi$$

from which the following is obtained:

$$J(\omega_n)=(\gamma_n{}^2-1)^{\frac{1}{2}}\left\{\frac{\pm\gamma_{cg}\left[\left(\frac{T_n}{M_nc^2}\right)^2+2\left(\frac{T_n}{M_nc^2}\right)\right]^{\frac{1}{2}}\mp\cos\omega_n\left(\frac{T_n}{M_nc^2}+1\right)(\gamma_{cg}{}^2-1)^{\frac{1}{2}}}{\left(\frac{T_n}{M_nc^2}\right)^2+2\left(\frac{T_n}{M_nc^2}\right)}\right\}. \tag{6}$$

The upper sign is used when $n=1$ and the lower when $n=2$.

Finally, ϕ may be expressed explicitly as a function of θ by equating the momentum components p_{y_n} in the c.m. system and obtaining

$$\sin\phi=\frac{M_1}{M_2}\frac{\left[\left(\frac{T_1}{M_1c^2}\right)^2+2\left(\frac{T_1}{M_1c^2}\right)\right]^{\frac{1}{2}}}{\left[\left(\frac{T_2}{M_2c^2}\right)^2+2\left(\frac{T_2}{M_2c^2}\right)\right]^{\frac{1}{2}}}\sin\theta \tag{7}$$

where the quadrant of ϕ is determined by the signs of $\cos\phi$ obtained from the result

$$\cos\phi=\frac{(\gamma_{cg}{}^2-1)^{\frac{1}{2}}\left(\frac{T_2}{M_2c^2}+1\right)-(\gamma_2{}^2-1)^{\frac{1}{2}}\cos\Omega}{\gamma_{cg}\left[\left(\frac{T_2}{M_2c^2}\right)^2+2\left(\frac{T_2}{M_2c^2}\right)\right]^{\frac{1}{2}}}.$$

Tables III, IV, and V were prepared on an IBM Electronic Data Processing Machine, Type 701. At the heading of each set of tables is given the reactions involved and the mass values (55W) used in the computation. The conversion factor for mass to energy is one mass unit = 931.160 Mev. The first column labeled θ gives the laboratory angle of the neutron. The headings of the other columns give the bombarding energy of the proton or deuteron in Mev. The numbers in the columns then give the neutron energy in Mev corresponding to angle, θ, and bombarding energy.

BIBLIOGRAPHY

34O. Oliphant, Harteck, and Rutherford, Proc. Roy. Soc. (London) **A144**, 692 (1934).
35A. K. D. Alexopoulos, Helv. Phys. Acta **8**, 601 (1935).
36B. T. W. Bonner and W. M. Brubaker, Phys. Rev. **49**, 19 (1936).
36K. Kempton, Browne, and Maasdorp, Proc. Roy. Soc. (London) **A157**, 386 (1936).
36L. R. Ladenburg and R. B. Roberts, Phys. Rev. **50**, 1190 (1936).
37A. Amaldi, Hafstad, and Tuve, Phys. Rev. **51**, 896 (1937).
37B. T. W. Bonner, Phys. Rev. **52**, 685 (1937).
37D. P. I. Dee and C. W. Gilbert, Proc. Roy. Soc. (London) **A163**, 265 (1937).
37K. Kruger, Shoupp, and Stallman, Phys. Rev. **52**, 678 (1937).
37L. R. Ladenburg and M. H. Kanner, Phys. Rev. **52**, 911 (1937).
37R. R. B. Roberts, Phys. Rev. **51**, 810 (1937).
38B. Baldinger, Huber, and Staub, Helv. Phys. Acta **11**, 245 (1938).
39A. H. Aoki, Proc. Phys.-Math. Soc. Japan **21**, 232 (1939).
39Z. Zinn, Seely, and Cohen, Phys. Rev. **56**, 260 (1939).
40B. H. H. Barschall and M. H. Kanner, Phys. Rev. **58**, 590 (1940).
40S. E. O. Salant and N. F. Ramsey, Phys. Rev. **57**, 1075 (1940).
41R. H. T. Richards, Phys. Rev. **60**, 167 (1941).
42A. Amaldi, Bocciarelli, Ferretti, and Trabacchi, Naturwiss. **30**, 582 (1942); Amaldi, Bocciarelli, and Trabacchi, Ricerca sci. **12**, 830 (1941); Amaldi, Bocciarelli, Ferretti, and Trabacchi, Ricerca sci. **13**, 502 (1942).
42T. H. Tatel, Phys. Rev. **61**, 450 (1942).
43B. Baker, Holloway, Schreiber, and King, LAMS 11 (unpublished).
44C. F. C. Champion and C. F. Powell, Proc. Roy. Soc. (London) **183**, 64 (1944).
44J. P. Jensen, Z. Physik **122** (Nos. 5–8) 387–400 (1944).
45S. R. Sherr, Phys. Rev. **68**, 240 (1945).
46B1. Bailey, Bennett, Bergstralh, Nuckolls, Richards, and Williams, Phys. Rev. **70**, 583 (1946).
46B2. Bennett, Mandeville, and Richards, Phys. Rev. **69**, 418–22 (1946).
46C1. J. H. Coon and H. H. Barschall, Phys. Rev. **70**, 592 (1946).
46C2. E. T. Clarke and J. W. Irvine, Jr., Phys. Rev. **70**, 893 (1946).
46D. N. N. Das Gupta and S. K. Ghosh, Revs. Modern Phys. **18**, 225 (1946).
46G. Graves, Graves, Coon, and Manley, Phys. Rev. **70**, 101 (1946).
46M. Manley, Coon, and Graves, Phys. Rev. **70**, 101 (1946).
47A. Ageno, Amaldi, Bocciarelli, and Trabacchi, Phys. Rev. **71**, 20 (1947).
47H. A. O. Hanson and J. L. McKibben, Phys. Rev. **72**, 673 (1947).
47K. E. D. Klema, Phys. Rev. **72**, 88 (1947).
47P. C. F. Powell and G. P. S. Occhialini in *Report of the International Conference on Fundamental Particles and Low Temperature* (Physical Society London, 1947), Vol. 1, p. 150.
47S1. W. Sleator, Jr., Phys. Rev. **72**, 207 (1947).
47S2. J. H. Smith, Phys. Rev. **71**, 32 (1947).
48B1. Blair, Freier, Lampi, Sleator, and Williams, Phys. Rev. **74**, 1599 (1948).

48B2. Bretscher, French, and Seidl, Phys. Rev. **73**, 815 (1948).
48F. A. P. French, Phys. Rev. **73**, 1474 (1948).
48K. E. J. Konopinski and E. Teller, Phys. Rev. **73**, 822–830 (1948).
48L. J. S. Laughlin and P. G. Kruger, Phys. Rev. **73**, 197 (1948).
48M. E. M. McMillan and H. F. York, Phys. Rev. **73**, 262 (1948).
49A. P. Ammiraju, Phys. Rev. **76**, 1421 (1949).
49B1. H. H. Barschall and R. F. Taschek, Phys. Rev. **75**, 1819 (1949).
49B2. Brueckner, Hartsough, Hayward, and Powell, Phys. Rev. **75**, 555 (1949).
49B3. B. P. Burtt, Nucleonics **5**, 28 (August, 1949).
49B4. E. Bretscher and A. P. French, Phys. Rev. **75**, 1154 (1949).
49C1. Cook, McMillan, Peterson, and Sewell, Phys. Rev. **75**, 7 (1949).
49C2. Curtis, Fowler, and Rosen, Rev. Sci. Instr. **20**, 388 (1949).
49C3. Carlson, Goldstein, Rosen, and Sweeney, Los Alamos Report LA 723 (unpublished).
49E. Erickson, Fowler, and Stovall, Phys. Rev. **76**, 1141 (1949).
49F. Falk, Creutz, and Seitz, Phys. Rev. **76**, 322 (1949).
49G1. Graves, Rodrigues, Goldblatt, and Meyer, Rev. Sci. Instr. **20**, 579 (1949).
49G2. J. C. Grosskreutz, Phys. Rev. **76**, 482 (1949).
49H1. Hanson, Taschek, and Williams, Revs. Modern Phys. **21**, 635 (1949).
49H2. Hadley, Kelly, Leith, Segrè, Wiegand, and York, Phys. Rev. **75**, 351 (1949).
49H3. G. T. Hunter and H. T. Richards, Phys. Rev. **76**, 1445 (1949).
49J1. P. Jensen, Arkiv Fysik **1**, 515 (1949).
49J2. Jarvis, Hemmendinger, Everhart, Gittings, and Taschek, Phys. Rev. **75**, 1361 (1949).
49N. Yoshihiro Nakano, Phys. Rev. **76**, 981 (1949).
49L. Lampi, Freier, and Williams, Phys. Rev. **76**, 188 (1949).
49T1. Taschek, Argo, Hemmendinger, and Jarvis, Phys. Rev. **76**, 325 (1949).
49T2. Taschek, Hemmindinger, and Jarvis, Phys. Rev. **75**, 1464(A) (1949).
49W. L. Wolfenstein, Phys. Rev. **75**, 342(A) (1949).
49Z. L. R. Zumwalt, Oak Ridge National Laboratory Document, ORNL-397 (1949).
50A1. Allen, Livesay, and Wilkinson, Proc. Cambridge Phil. Soc. **46**, (PT 11) 339 (1950).
50A2. D. L. Allan and M. J. Poole, Proc. Roy. Soc. (London) **A204**, 488 (1950).
50A3. D. L. Allan and M. J. Poole, Proc. Roy. Soc. (London) **A204**, 500 (1950).
50B1. Beiduk, Pruett, and Konopinski, Phys. Rev. **77**, 622 (1950).
50B2. E. Bretscher and E. B. Martin, Helv. Phys. Acta **23** (Nos. 1–2), 15 (1950).
50D. J. Dejuren and N. Knable, Phys. Rev. **77**, 606 (1950).
50F. J. L. Fowler and J. M. Slye, Jr., Phys. Rev. **77**, 787 (1950).
50G. S. N. Ghoshal, Phys. Rev. **80**, 939 (1950).
50H. R. H. Hildebrand and C. E. Leith, Phys. Rev. **80**, 842 (1950).
50J. Jarvis, Hemmendinger, Argo, and Taschek, Phys. Rev. **79**, 929 (1950).
50L. K. Lintner, Ost. Akad. Wiss. Abt. 11A **158**, 135–68 (1950).
50M. McNeill, Thoneman, and Price, Nature **166**, 28 (1950).
50N. Nuclear Data Circular of National Bureau of Standards **499** (1950).
50P1. Pruett, Beiduk, and Konopinski, Phys. Rev. **77**, 628 (1950).
50P2. D. Phillips, private communication, LASL.
50S. Sanders, Moffatt, and Roaf, Phys. Rev. **77**, 754 (1950).
50W. H. Waffler, Helv. Phys. Acta **23** (Nos. 1–2), 239 (1950).
51A1. Aron, Hoffman, and Williams, AECU 663 (unpublished) (1951).
51A2. Allred, Phillips, and Rosen, Phys. Rev. **82**, 782 (1951).
51A3. J. C. Allred, Phys. Rev. **84**, 695 (1951).
51A4. Allen, Nechaj, Sun, and Jennings, Phys. Rev. **81**, 536 (1951).
51B1. S. T. Butler and J. L. Symonds, Phys. Rev. **83**, 858 (1951).
51B2. Brolley, Coon, and Fowler, Phys. Rev. **82**, 190 (1951).
51B3. E. M. Baldwin, Phys. Rev. **83**, 495 (1951).
51B4. Brolley, Fowler, and Stovall, Phys. Rev. **82**, 502 (1951).
51B5. N. Bloembergen and P. J. Van Heerden, Phys. Rev. **83**, 561 (1951).
51B6. T. W. Bonner and J. W. Butler, Phys. Rev. **83**, 1091 (1951).
51B7. R. J. Blin-Stoyle, Proc. Roy. Soc. (London) **A64**, 700 (1951).
51B8. Blaser, Boehm, Marimer, and Peaslee, Helv. Phys. Acta **24**, 3–38 (1951).
51B9. Blaser, Boehm, Marimer, and Scherrer, Helv. Phys. Acta **24**, 441 (No. 5) (1951).
51B10. Blaser, Boehm, Marimer, and Scherrer, Helv. Phys. Acta **24**, 465 (No. 5) (1951).
51C1. W. F. Caplehorn and G. P. Rundle, Proc. Phys. Soc. (London) **A64**, 546 (1951).
51C2. B. L. Cohen, Phys. Rev. **81**, 184 (1951).
51C3. B. L. Cohen and C. E. Falk, Phys. Rev. **84**, 173 (1951).
51F1. B. H. Flowers, Proc. Roy. Soc. (London) **A204**, 503 (1951).
51F2. C. E. Falk, Phys. Rev. **83**, 499 (1951).
51G. P. C. Gugelot, Phys. Rev. **81**, 51 (1951).
51H. J. Hughes, Proc. Phys. Soc. (London) **A64**, 797 (1951).
51L1. A. H. Lasday, Phys. Rev. **81**, 139 (1951).
51L2. A. B. Lillie and J. P. Conner, Rev. Sci. Instr. **22**, 210 (1951).
51S1. J. Sharpe and G. H. Stafford, Proc. Phys. Soc. (London) **A64**, 211 (1951).
51S2. L. W. Smith and P. G. Kruger, Phys. Rev. **83**, 1137 (1951).
51T. Taylor, Pickavance, Cassels, and Randle, Phil. Mag. **42**, 328 (1951).
51W. Roger Wallace, Phys. Rev. **81**, 443 (1951).
52A1. AECU-2040 (1952) (unpublished).
52A2. Argo, Taschek, Agnew, Hemmendinger, and Leland, Phys. Rev. **87**, 612 (1952).
52B1. Barshall, Rosen, Taschek, and Williams, Revs. Modern Phys. **24**, 1 (1952).
52B2. H. H. Barschall, Revs. Modern Phys. **24**, 120 (1952).
52B3. R. J. Blin-Stoyle, Proc. Phys. Soc. (London) **A65**, 949 (1952).
52B4. Brolley, Fowler, and Schlacks, Phys. Rev. **88**, 618 (1952).
52B5. J. M. Blatt and V. F. Weisskopf, *Theoretical Nuclear Physics* (John Wiley and Sons, Inc., New York, 1952).
52B6. Bishop, Westhead, and Halban, Nature **170**, 113 (1952).
52C1. Coon, Graves, and Barschall, Phys. Rev. **88**, 562 (1952).
52C2. W. G. Cross, Phys. Rev. **87**, 223 (1952).
52C3. Conner, Bonner, and Smith, Phys. Rev. **88**, 468 (1952).
52D. E. der Mateosian and A. Smith, Phys. Rev. **87**, 193 (1952).
52F1. S. G. Forbes, Phys. Rev. **88**, 1309 (1952).
52F2. M. Fierz, Helv. Phys. Acta **25**, 629 (1952).
52G. L. S. Goodman, Phys. Rev. **88**, 686 (1952).
52H. E. L. Hubbard and K. R. MacKenzie, Phys. Rev. **85**, 107 (1952).
52L. Longley, Little, and Slye, Phys. Rev. **86**, 419 (1952).
52M1. Mott, Guernsey, and Nelson, Phys. Rev. **88**, 9 (1952).
52M2. R. F. Mozley and F. C. Shoemaker, Rev. Sci. Instr. **23**, 569 (1952).
52M3. H. C. Martin and B. C. Diven, Phys. Rev. **86**, 565 (1952).

52P. Poss, Salant, Snow, and Yuan, Phys. Rev. **87**, 11 (1952).
52S. T. F. Stratton and G. C. Freier, Phys. Rev. **88**, 261 (1952).
53A1. Allred, Armstrong, and Rosen, Phys. Rev. **91**, 90 (1953).
53A2. S. K. Allison and S. D. Warshaw, Revs. Modern Phys. **25**, 779 (1953).
53B1. J. Benveniste and B. Cork, Phys. Rev. **89**, 422 (1953).
53B2. J. E. Brolley, Jr., Phys. Rev. **89**, 877 (1953).
53B3. E. Baumgartner and P. Huber, Helv. Phys. Acta **26**, 545 (1953).
53D1. R. B. Day and R. L. Henkel, Phys. Rev. **92**, 358 (1953).
53D2. W. C. Dickinson and D. C. Dodder, Rev. Sci. Instr. **24**, 428 (1953).
53D3. Dunbar, Reynolds, Wenzel, and Whaling, Phys. Rev. **91**, 496(A) (1953). Data in 53A2.
53E1. *Experimental Nuclear Physics* (John Wiley and Sons, Inc., New York, 1953), B. T. Feld, Vol. II, p. 426.
53E2. *Experimental Nuclear Physics* (John Wiley and Sons, Inc., New York, 1953), H. A. Bethe and Julius Ashkin, Vol. I, p. 243.
53G. J. H. Gammel, Phys. Rev. **92**, 1092 (1953).
53H. Hafner, Hornyak, Falk, Snow, and Coor, Phys. Rev. **89**, 204 (1953).
53L. R. W. Lamphere, Phys. Rev. **91**, 655 (1953).
53M. H. C. Martin and R. F. Taschek, Phys. Rev. **89**, 1302 (1953).
53N1. N. Nereson and S. Darden, Phys. Rev. **89**, 775 (1953).
53N2. V. Nedzel, Phys. Rev. **90**, 169 (1953).
53P. E. B. Paul and R. L. Clarke, Can. J. Phys. **31**, 267 (1953).
53R1. Remley, Jentschke, and Kruger, Phys. Rev. **89**, 1194 (1953).
53R2. L. Rosen, Nucleonics **11**, 38 (1953).
53S1. Selove, Strauch, and Titus, Phys. Rev. **92**, 724 (1953).
53S2. A. Simon and T. A. Welton, Phys. Rev. **90**, 1036 (1953).
53S3. A. Simon, Phys. Rev. **92**, 1050 (1953).
53T. A. E. Taylor and E. Wood, Phil. Mag. **44**, 95 (1953).
53W. Willard, Bair, and Kington, Phys. Rev. **90**, 865 (1953).
53Y. Yarnell, Lovberg, and Stratton, Phys. Rev. **90**, 292 (1953).
54A1. H. Argo, private communication, LASL, 1954.
54A2. Adair, Darden, and Fields, Phys. Rev. **96**, 503 (1954).
54A3. Arnold, Phillips, Sawyer, Stovall, and Tuck, Phys. Rev. **93**, 483 (1954).
54B. J. R. Beyster and M. Walt, private communication, LASL, 1954.
54C1. C. F. Cook and T. W. Bonner, Phys. Rev. **94**, 651 (1954).
54C2. O. Chamberlain and J. W. Easley, Phys. Rev. **94**, 208 (1954).
54C3. L. Cranberg, private communication.
54C4. Chilton, Cooper, and Harris, Phys. Rev. **93**, 413 (1954).
54F1. W. M. Fairbairn, Proc. Phys. Soc. (London) **A67**, 990 (1954).
54F2. Fields, Becker, and Adair, Phys. Rev. **94**, 389 (1954).
54F3. R. G. Freemantle, private communication to W. M. Fairbairn, and data published in Proc. Phys. Soc. (London) **A67**, 990 (1954).
54H. Henkel, Smith, and Perry, LASL private communication.
54J. G. Jarvis, private communication, LASL.
54M1. McCrary, Taylor, and Bonner, Phys. Rev. **94**, 808 (1954).
54M2. H. C. Martin, LASL private communication.
54M3. Meier, Scherrer, and Trumpy, Helv. Phys. Acta **27**, 577 (1954).
54O. G. K. O'Neill, Phys. Rev. **95**, 635 (1954).
54P. J. Perry, Jr., LASL, private communication.
54R1. F. L. Ribe and J. D. Seagrave, Phys. Rev. **94**, 934 (1954).
54R2. L. Rosen, LASL, private communication.
54S1. R. H. Stahl and N. F. Ramsey, Phys. Rev. **96**, 1310 (1954).
54S2. C. W. Snyder and V. E. Parker, Phys. Rev. **95**, 635 (1954).
54S3. R. K. Smith and J. E. Perry, LASL, private communication.
54S4. J. R. Smith, Phys. Rev. **95**, 730 (1954).
54T. C. C. Trail and C. H. Johnson, Phys. Rev. **95**, 1363 (1954).
54V. D. M. Van Patter and W. Whaling, Revs. Modern Phys. **26**, 402 (1954).
54W1. M. C. Walske, private communication, LASL, 1954.
54W2. Willard, Bair, and Kington, Phys. Rev. **95**, 1359 (1954).
55A1. A. J. Allen, private communication, University of Pittsburgh, 1955.
55B1. J. E. Brolley, Jr., and F. L. Ribe, Phys. Rev. **98**, 1112 (1955).
55B2. L. Blumberg and S. I. Schlesinger, AECU 3118.
55C. B. L. Cohen, Phys. Rev. **98**, 1206 (1955).
55G1. A. Galonsky and John Judish, Phys. Rev. **98**, 1168 (1955).
55H1. A. Hemmendinger and H. V. Argo, Phys. Rev. **98**, 70 (1955).
55H2. Henkel, Perry, and Smith, Phys. Rev. **99**, 1050 (1955).
55S. J. D. Seagrave, Phys. Rev. **97**, 757 (1955).
55W. A. H. Wapstra, Physica **21**, 367, (1955).